CHALMERS
UNIVERSITY OF TECHNOLOGY

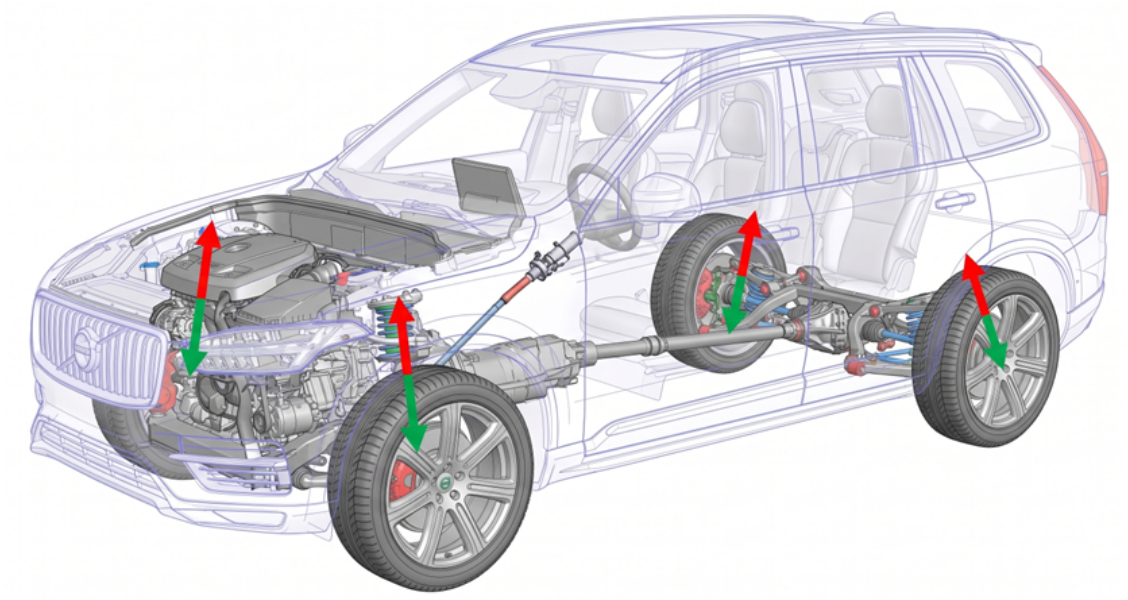

Roll motion control with a fully active suspension system

High-Level Motion Control and Low-Level Actuator Implementation

Master's thesis in the Master's Programme Systems, Control and Mechatronics

Soheb Kanon
Yiming Li

Department of Mechanics and Maritime Sciences
CHALMERS UNIVERSITY OF TECHNOLOGY
Gothenburg, Sweden 2026
www.chalmers.se

Degree project report 2026

Roll motion control with a fully active suspension system

High-Level Motion Control and Low-Level Actuator Implementation

Soheb Kanon
Yiming Li

CHALMERS
UNIVERSITY OF TECHNOLOGY

Department of Mechanics and Maritime Sciences
Chalmers University of Technology
Gothenburg, Sweden 2026

Roll motion control with a fully active suspension system
High-Level Motion Control and Low-Level Actuator Implementation
SOHEB KANON
YIMING LI

Supervisors: Lars Drugge, Yansong Huang, Bengt Jacobson
Examiner: Bengt Jacobson, Vehicle Dynamics and Autonomous Systems

Degree project report 2026
Department of Mechanics and Maritime Sciences,
Chalmers University of Technology
SE-412 96 Gothenburg
Sweden
Telephone +46 31 772 1000

Cover: Illustration of a passenger vehicle equipped with a fully active suspension system.

Typeset in LaTeX
Gothenburg, Sweden 2026

Roll motion control with a fully active suspension system
High-Level Motion Control and Low-Level Actuator Implementation
SOHEB KANON
YIMING LI
Department of Mechanics and Maritime Sciences
Chalmers University of Technology

Abstract

During cornering, vehicle roll motion directly affects lateral load transfer, tire force distribution, and handling consistency. This thesis therefore investigates roll-gradient shaping for a fully active suspension system in simulated cornering maneuvers and driver-in-the-loop tests, with emphasis on how body-level roll objectives can be realized through actuator-level force generation.

The proposed method combines a high-level body-motion controller with a low-level hydraulic actuator controller. At the high level, lateral acceleration is estimated from vehicle speed and steering input and used to generate a feedforward roll moment, while proportional-integral (PI) feedback is applied to roll, pitch, and heave states. The resulting generalized force and moment targets are transformed into corner suspension-force commands through a pseudoinverse force-allocation method. At the low level, the required damper forces are converted into continuously controlled damper (CCD) current commands and motor-pump unit (MPU) flow-rate commands using supplier-based lookup tables and mode-switching logic.

The controller is implemented in MATLAB/Simulink and evaluated in both IPG CarMaker and the VI-CRT driver-in-the-loop real-time simulator. In CarMaker, the proposed controller tracks prescribed roll-gradient targets and produces suspension-force distributions that remain consistent with the intended vehicle behavior. The low-level controller also shows satisfactory force-tracking performance, with the main deviations appearing near rapid force reversals. In the VI-CRT simulator, the controller preserves the expected roll characteristics over a wide lateral acceleration range under real-time driving conditions, despite driver input variability and transient steering effects.

Overall, the results show that roll-motion control for a fully active suspension system should be evaluated as a connected body-level and actuator-level problem. High-level motion objectives and low-level actuator behavior must therefore be considered together when evaluating active suspension concepts.

Keywords: Fully Active Suspension, Roll Motion Control, Vehicle Dynamics, Hierarchical Control, Hydraulic Actuators, Force Allocation

Reflections

This work points to a familiar engineering trade-off. Better roll control can improve both stability and perceived comfort, especially in situations where a large body roll would otherwise reduce driver confidence or increase the risk of loss of control. For that reason, active suspension is not only a comfort feature; it can also affect vehicle safety.

At the same time, the added control authority does not come for free. A fully active suspension system brings extra hardware, higher energy use, more complicated actuation, and a harder implementation problem. In practice, that means any performance gain has to be judged against cost, power demand, reliability, and maintainability.

What stands out most in this thesis is that control performance alone is not enough. A roll-control concept may look convincing at the body-motion level and still become much less attractive once actuator behavior and implementation constraints are included. That is why the connection between high-level objectives and low-level feasibility is central to the whole problem.

Acknowledgements

We would like to express our sincere gratitude to everyone who supported us throughout the completion of this master's thesis.
First, we would like to thank Volvo Cars for providing us with the opportunity to conduct this thesis in collaboration with the company. We are especially grateful to our supervisor at Volvo Cars, Yansong Huang, for his valuable guidance, support, and continuous feedback during the project. We would also like to thank Erik Andersson, Oskar Malm, Stavros Angelis, and Akshay Naik for their assistance and for sharing their knowledge and expertise throughout the course of this work.
We would also like to express our sincere appreciation to Lars Drugge at KTH Royal Institute of Technology, and to Bengt Jacobson at Chalmers University of Technology, for their insightful discussions, constructive feedback, and academic guidance throughout the thesis process.
Finally, we would like to thank our families and friends for their continuous encouragement, patience, and support throughout our studies and during the completion of this thesis.

Soheb Kanon, Yiming Li, Gothenburg, June 2026

List of Acronyms

Below is the list of acronyms that have been used throughout this thesis listed in alphabetical order:

ARB	anti-roll bar
CMC	Center of mass of the chassis
DOF	Degree of freedom
FAS	Fully active suspension
FL	Front-left
FR	Front-right
IDT	Input decoupling transformation
IPG	IPG Automotive
LQR	Linear quadratic regulator
LPV	Linear Parameter-Varying
MPC	Model predictive control
MPU	Motor-pump unit
MR	Motion ratio
PI	Proportional-integral
PID	Proportional-integral-derivative
RL	Rear-left
RR	Rear-right
SDG	Sustainable Development Goal
VI-CRT	VI-CarRealTime

Contents

List of Figures

List of Tables

1

Introduction

A suspension system is a critical subsystem in automobiles, directly influencing ride comfort, road holding, and vehicle stability [1]. Conventional passive suspension systems inherently involve a strict compromise: a soft suspension reduces vehicle body accelerations to improve ride comfort, while a stiff suspension is required to improve tire–road contact and handling dynamics [2]. To overcome these physical limitations, active suspension systems have been developed. By using actuators to generate real-time controllable forces, active suspension systems can adapt to changing road and driving conditions, thereby reducing vibrations and improving vehicle body-motion control compared with conventional passive systems [3], [4].

Among the different vehicle body motions, roll dynamics play a particularly important role in vehicle safety and handling [5]. During cornering manoeuvres or rapid lane changes, lateral acceleration generates load transfer between the left and right wheels, producing a significant rolling moment [5]. Excessive roll motion can deteriorate passenger comfort and may also compromise vehicle stability, increasing the risk of rollover in critical manoeuvres [6]. Consequently, active suspension systems specifically designed for roll-motion control have become a relevant research topic in advanced automotive engineering [4], [6].

1.1 Background

Advanced vehicle dynamics models have been widely developed to analyse suspension performance and vehicle body motions. In addition to simplified models such as quarter-car and half-car representations, more comprehensive full-vehicle models have been proposed to capture the interactions between vehicle subsystems. A commonly used representation is the seven-degree-of-freedom (7-DOF) vehicle model, which describes the heave, pitch, and roll motions of the sprung mass together with the vertical motions of the four unsprung masses.

Beyond this foundational representation, researchers have developed higher-order and nonlinear full-vehicle models to capture more complex suspension characteristics and to evaluate performance under demanding driving conditions and extreme manoeuvres [7], [8].

Based on such vehicle models, a wide range of control strategies have been proposed to improve vehicle stability and ride performance. In particular, advanced control approaches have been investigated to achieve coordinated or decoupled control of vehicle body motions, allowing heave, pitch, and roll responses to be regulated either jointly or independently [9].

To address issues such as actuator delays and rapid transient dynamics during aggressive steering manoeuvres, feedforward control strategies are often combined with conventional feedback control architectures. These approaches enable the suspension system to respond more effectively to dynamic driving conditions and help reduce excessive body roll and potential rollover risks [10].

Therefore, the development of robust and computationally efficient control algorithms based on comprehensive vehicle dynamic models remains an important challenge for active suspension systems. In particular, effective roll-motion control requires not only vehicle-level control design, but also actuator-level implementation capable of realizing the requested suspension forces in real time.

1.2 Purpose

The purpose of this project is to investigate the performance of a fully active suspension system for a passenger vehicle. The study focuses on the design and evaluation of active control strategies for improving vehicle roll behavior and stability under representative driving and road conditions.

1.3 Research Questions

Based on the purpose of this thesis, the following research questions are formulated:

- RQ1: How can a high-level controller be designed to generate suspension force requests for shaping vehicle roll behavior according to prescribed roll gradient targets?
- RQ2: How can a low-level actuator controller be designed to convert the requested suspension forces into feasible damper-valve and motor-pump commands?
- RQ3: How accurately can the proposed fully active suspension control system track positive, zero, and negative roll-gradient targets under predefined CarMaker maneuvers and driver-in-the-loop VI-CRT operation?

1.4 Research Objectives

The main objective of this project is to design and evaluate a fully active suspension control system for a passenger vehicle, with particular emphasis on roll-motion control and actuator-level implementation. To achieve this objective, the work is structured as follows:

- Develop a high-level controller that computes requested suspension forces from vehicle-state information for roll, pitch, and heave regulation.
- Develop a low-level controller that converts force requests into actuator-level commands for the motor-pump and damper valve system.

- Implement and evaluate the complete control architecture in MATLAB/Simulink using IPG CarMaker scenarios.
- Validate the real-time behavior of the controller in the VI-CRT simulator under driver-in-the-loop operation.

1.5 Limitations

- This project focuses only on the Volvo XC_90 T8 model year 2020 platform; therefore, the developed control strategy may not be directly applicable to other vehicle models without further modification.
- The interaction between rebound and compression behavior in the suspension actuator is simplified and not modeled in full detail.
- The fluid flow within the suspension system is assumed to be ideal, meaning that flow losses and pressure drops caused by internal components are neglected.
- The valve, motor, and pump components are represented with simplified models; parameter uncertainties and unmodeled dynamics are not fully captured.
- The change in valve opening is assumed to occur instantaneously and with perfect accuracy.
- Sensor measurements are assumed to be ideal and noise-free, particularly within the simulation environment.
- The system is evaluated under a limited set of predefined driving scenarios and road profiles in simulation and real-time simulator testing, so it is not assessed under all possible real-world conditions.
- The main focus of this project is the development of a control strategy for reducing vehicle roll motion in steady-state. Pitch and heave motions are not the primary focus of the study.

  Quantitative evaluation of energy consumption is outside the scope of this thesis.

1.6 Related Work

Active suspension control has been widely studied to improve vehicle ride comfort, road holding, and handling stability [11], [12]. Early studies and surveys emphasized classical model-based approaches such as PID and LQR, while later works also explored robust and adaptive schemes, including H_∞-oriented and backstepping-based designs [11], [13]. These approaches rely on mathematical models of the suspension system and aim to regulate suspension forces to reduce body vibration and improve tire-road contact [12]. Model predictive control has also been applied to

semi-active full-vehicle suspension control, where actuator constraints and real-time implementation are important considerations [14].

In addition to vertical dynamics, vehicle roll motion has attracted significant attention due to its direct influence on handling stability and rollover prevention. During cornering, lateral acceleration acting at the height of the centre of gravity creates a roll moment that causes lateral load transfer between the left and right wheels, even in the absence of significant body roll motion. To mitigate these effects, roll moment control strategies have been developed, where suspension actuators generate counteracting moments to reduce body roll [15].

Classical control approaches such as PID controllers are widely used in suspension systems due to their simplicity and robustness. These controllers are often employed to regulate roll angle, roll rate, or suspension forces. However, purely feedback-based controllers may suffer from delays and limited performance during rapid transient manoeuvres.

To address these limitations, feedforward and preview-based control strategies have been proposed. These methods utilize measurable inputs such as steering angle or lateral acceleration to anticipate vehicle dynamics and improve control response [16].

In practical implementations, actuator dynamics play a crucial role in active suspension systems. Electro-hydraulic actuators introduce nonlinear dynamics and force-tracking constraints that must be handled by dedicated low-level control strategies [17], [18]. For pump-based hydraulic active suspension systems, actuator sizing, motor-pump operation, and actuator dynamic response also directly affect the achievable control performance [19].

Surveys of active and semi-active suspension control show that actuator constraints and implementation details significantly influence closed-loop performance [3], [11]. Comparative studies on semi-active suspension control further highlight the role of implementation constraints and performance trade-offs [20]. In practical controller design, this motivates multi-layer architectures in which high-level body-motion objectives are translated into low-level actuator commands.

A key practical challenge is therefore to ensure that roll-moment commands generated at the vehicle-motion level can be realized by the hydraulic actuator system under its nonlinear mapping and operating constraints. This motivates the development of an integrated control framework combining high-level roll-moment control with low-level actuator management, which is the focus of this work.

1.7 Ethical and Sustainability Aspects

Improved roll control can contribute to road safety and occupant well-being, supporting SDG 3 (Good Health and Well-being) and SDG 11 (Sustainable Cities and Communities) [21]. By reducing the risk of loss-of-control and rollover in emergency maneuvers, active suspension and roll motion control can lower accident severity and frequency, especially for vehicles with high centers of gravity or heavy loads [6], [15].

Fully active suspension systems, however, introduce additional hardware, complexity, and energy consumption [3], [19]. This has implications for resource use,

manufacturing impact, and end-of-life recycling (SDG 12, Responsible Consumption and Production), as well as for vehicle energy efficiency and emissions (SDG 13, Climate Action) [21]. These trade-offs should be considered when assessing the practical applicability of fully active suspension systems. Although actuator energy usage is an important aspect, a quantitative evaluation of energy consumption is outside the scope of this thesis.

Advanced suspension systems tend to appear first in premium vehicles, which raises questions about equity and accessibility. At the same time, the knowledge gained on control design and trade-offs can inform future implementations in higher-volume segments. The thesis will reflect on these aspects and on how active suspension technology can be developed and deployed in a way that balances safety, comfort, energy use and resource efficiency. Data privacy is not expected to be a major issue, since the work focuses on physical vehicle behavior rather than personal data.

2

Vehicle models

This chapter presents the vehicle models used in this thesis. It first introduces the quarter-car model as the basic representation of vertical suspension dynamics and then formulates the seven-degree-of-freedom full-car active suspension model. A single-track (bicycle) model for steady-state cornering is then introduced to support lateral-acceleration estimation from steering input and vehicle speed. The chapter finally describes the suspension and damper modeling assumptions used in the control design.

2.1 Quarter-Car Suspension Model

Quarter-car suspension model is considered the simplest model for representing a vehicle suspension system. It simplifies the vertical dynamics by representing only one vehicle corner instead of modeling all four corners in a full-car model.

In this model, the vehicle is divided into two main parts: the sprung mass and the unsprung mass. The sprung mass represents the part of the vehicle supported by the suspension system and accounts for most of the vehicle body. The unsprung mass represents the parts that are not supported by the suspension, such as the wheel, tire, and related components.

The connection between the sprung and unsprung masses is simplified and modelled using a spring and a damper. These elements represent the suspension system. As shown in Table 2.1 and Fig. 2.1, this simplified model provides a basic representation of the suspension behaviour.

Table 2.1: Description of the parameters used in the passive quarter-car model.

Symbol	**Quantity**	**Unit**
k_s	Spring constant	N/m
k_t	Tire spring constant	N/m
m_s	Sprung mass	kg
m_u	Unsprung mass	kg
b_s	Damping coefficient	N s/m
z_s	Vertical displacement of sprung mass (heave)	m
z_u	Vertical displacement of unsprung mass	m
z_r	Vertical displacement of road	m

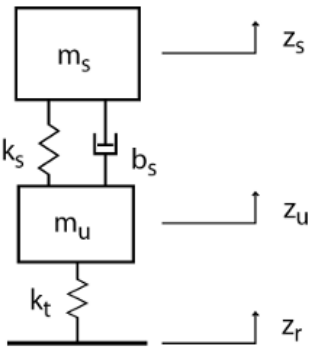

Figure 2.1: Passive quarter-car suspension model.

The force balance of the sprung and unsprung masses can be written as

$$m_s\ddot{z}_s = F_s + F_d, \tag{2.1}$$
$$m_u\ddot{z}_u = F_t - F_s - F_d, \tag{2.2}$$

where F_s, F_d, and F_t denote the suspension spring force, damper force, and tire force, respectively. With the positive vertical direction defined upward, these forces are modeled as

$$F_s = k_s(z_u - z_s), \tag{2.3}$$
$$F_d = b_s(\dot{z}_u - \dot{z}_s), \tag{2.4}$$
$$F_t = k_t(z_r - z_u). \tag{2.5}$$

2.2 Full-Car Active Suspension Model Formulation

Full-car active suspension model considered in this thesis is a linearized seven-degree-of-freedom model. It consists of the heave, pitch, and roll motions of the sprung mass together with the vertical motions of the four unsprung masses. The active suspension is represented by four controllable suspension corner forces, which are later used in the force-allocation step and subsequently converted into damper-side force commands through the suspension motion ratio.

The symbols used in the full-car model are summarized in Table 2.2.

The geometric parameters l_f and l_r denote the longitudinal distances from the vehicle center of gravity to the front and rear axles, respectively. Their sum defines the wheelbase,

$$L = l_f + l_r. \tag{2.6}$$

The parameters t_l and t_r denote the lateral distances from the center of gravity to the left and right suspension corners, respectively.

A schematic of the modeled system is shown in Fig. 2.2.

Table 2.2: Symbols used in the full-car model with active suspension.

Symbol	Quantity	Unit
z	Body vertical displacement (heave)	m
θ	Body pitch angle	rad
ϕ	Body roll angle	rad
$z_{u,ij}$	Unsprung-mass vertical displacement at corner ij, $ij \in \{fl, fr, rl, rr\}$	m
$z_{r,ij}$	Road input at corner ij, $ij \in \{fl, fr, rl, rr\}$	m
m_s	Sprung mass	kg
$m_{u,ij}$	Unsprung mass at corner ij, $ij \in \{fl, fr, rl, rr\}$	kg
k_f	Front suspension spring stiffness	N/m
k_r	Rear suspension spring stiffness	N/m
b_f	Front suspension damping coefficient	N s/m
b_r	Rear suspension damping coefficient	N s/m
k_{tf}	Front tire stiffness	N/m
k_{tr}	Rear tire stiffness	N/m
I_x	Roll mass moment of inertia	kg m^2
I_y	Pitch mass moment of inertia	kg m^2
l_f	Distance from center of gravity to front axle	m
l_r	Distance from center of gravity to rear axle	m
t_l	Left lateral distance from center of gravity	m
t_r	Right lateral distance from center of gravity	m
L	Wheelbase, $L = l_f + l_r$	m
f_{ij}	Controllable suspension corner force at corner ij, $ij \in \{fl, fr, rl, rr\}$	N
$F_{t,ij}$	Tire vertical force at corner ij, $ij \in \{fl, fr, rl, rr\}$	N
$z_{s,ij}$	Sprung-mass corner displacement at corner ij, $ij \in \{fl, fr, rl, rr\}$	m
Δ_{ij}	Relative suspension deflection at corner ij, $ij \in \{fl, fr, rl, rr\}$	m

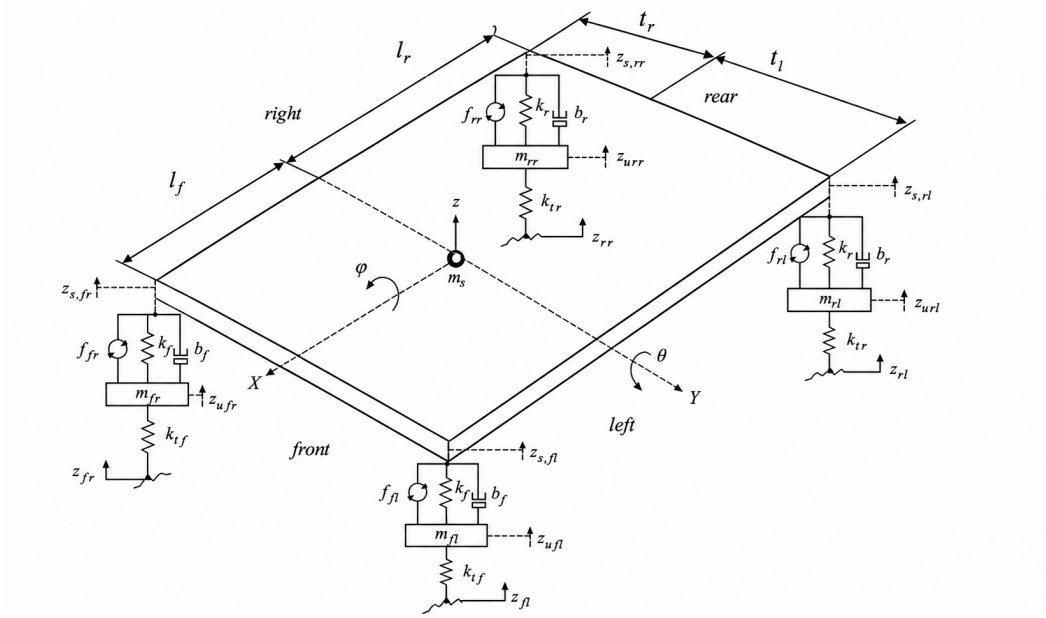

Figure 2.2: full car model with all Seven-degree-of-freedom [9].

2.2.1 Model Assumptions

- Positive vertical displacement is upward.
- Pitch and roll angles are small, and the model is linearized about the static equilibrium position.
- Suspension springs and dampers are modeled as linear elements with constant parameters.
- Tire dynamics are represented by linear vertical stiffness terms, while tire damping is neglected.
- Road excitations are modeled as vertical inputs at the four wheel contact points.
- The active suspension acts through equivalent controllable suspension corner forces f_{ij}.

The vertical displacement of the sprung mass at each suspension corner is written as

$$z_{s,fl} = z - l_f\theta + t_l\phi, \tag{2.7}$$
$$z_{s,fr} = z - l_f\theta - t_r\phi, \tag{2.8}$$
$$z_{s,rl} = z + l_r\theta + t_l\phi, \tag{2.9}$$
$$z_{s,rr} = z + l_r\theta - t_r\phi. \tag{2.10}$$

The corresponding relative suspension deflections are

$$\Delta_{fl} = z_{s,fl} - z_{u,fl}, \tag{2.11}$$
$$\Delta_{fr} = z_{s,fr} - z_{u,fr}, \tag{2.12}$$
$$\Delta_{rl} = z_{s,rl} - z_{u,rl}, \tag{2.13}$$
$$\Delta_{rr} = z_{s,rr} - z_{u,rr}. \tag{2.14}$$

The tire vertical forces are expressed as

$$F_{t,fl} = k_{tf}\left(z_{r,fl} - z_{u,fl}\right), \tag{2.15}$$
$$F_{t,fr} = k_{tf}\left(z_{r,fr} - z_{u,fr}\right), \tag{2.16}$$
$$F_{t,rl} = k_{tr}\left(z_{r,rl} - z_{u,rl}\right), \tag{2.17}$$
$$F_{t,rr} = k_{tr}\left(z_{r,rr} - z_{u,rr}\right). \tag{2.18}$$

The suspension forces acting on the sprung mass at the four corners are defined as

$$F_{s,fl} = -k_f\Delta_{fl} - b_f\dot{\Delta}_{fl} + f_{fl}, \tag{2.19}$$
$$F_{s,fr} = -k_f\Delta_{fr} - b_f\dot{\Delta}_{fr} + f_{fr}, \tag{2.20}$$
$$F_{s,rl} = -k_r\Delta_{rl} - b_r\dot{\Delta}_{rl} + f_{rl}, \tag{2.21}$$
$$F_{s,rr} = -k_r\Delta_{rr} - b_r\dot{\Delta}_{rr} + f_{rr}. \tag{2.22}$$

The heave motion of the sprung mass is then given by

$$m_s\ddot{z} = F_{s,fl} + F_{s,fr} + F_{s,rl} + F_{s,rr}. \tag{2.23}$$

The roll motion of the sprung mass is written as

$$I_x\ddot{\phi} = t_l\left(F_{s,fl} + F_{s,rl}\right) - t_r\left(F_{s,fr} + F_{s,rr}\right). \tag{2.24}$$

The pitch motion of the sprung mass is written as

$$I_y\ddot{\theta} = -l_f\left(F_{s,fl} + F_{s,fr}\right) + l_r\left(F_{s,rl} + F_{s,rr}\right). \tag{2.25}$$

The vertical dynamics of the four unsprung masses are expressed as

$$m_{u,fl}\ddot{z}_{u,fl} = -F_{s,fl} + F_{t,fl}, \tag{2.26}$$
$$m_{u,fr}\ddot{z}_{u,fr} = -F_{s,fr} + F_{t,fr}, \tag{2.27}$$
$$m_{u,rl}\ddot{z}_{u,rl} = -F_{s,rl} + F_{t,rl}, \tag{2.28}$$
$$m_{u,rr}\ddot{z}_{u,rr} = -F_{s,rr} + F_{t,rr}. \tag{2.29}$$

2.3 Single-Track Bicycle Model for Steady-State Cornering

In addition to the vertical suspension models introduced above, a bicycle model is used to describe the planar vehicle motion required for lateral-acceleration estimation. The purpose of this model is not to capture detailed suspension dynamics, but

to provide a simple relationship between vehicle speed, steering input, and lateral acceleration during steady-state cornering.

In the bicycle-model approximation, the left and right wheels on each axle are replaced by a single equivalent front wheel and a single equivalent rear wheel. The vehicle is assumed to move at constant longitudinal speed along a circular path of radius R on a flat road. Small steering and slip angles are assumed. In a real vehicle, the left and right front wheels generally follow Ackermann steering geometry, but in the present analysis they are represented by a single equivalent front-wheel steering angle δ. If the available steering input is the steering-wheel angle δ_{sw}, the equivalent front-wheel steering angle is obtained through the steering ratio i_s as

$$\delta = \frac{\delta_{sw}}{i_s}. \tag{2.30}$$

Therefore, Ackermann steering is not modeled explicitly in this thesis.

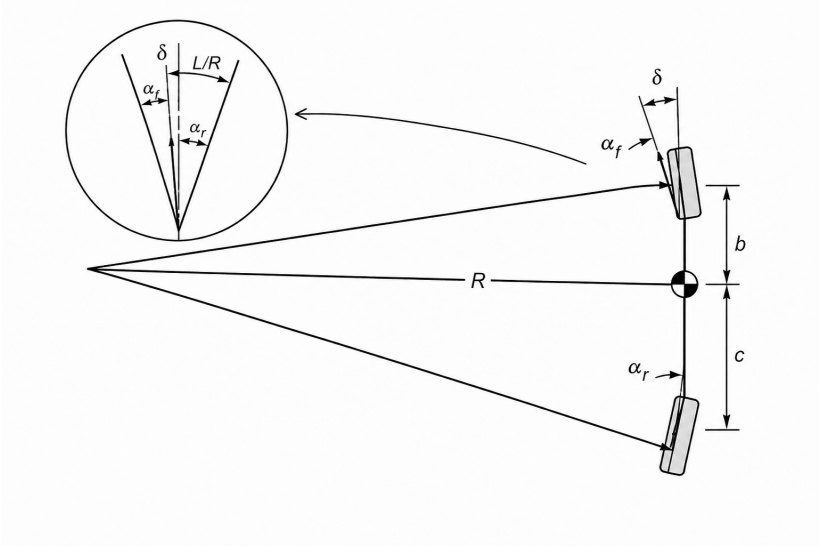

Figure 2.3: Steady-state cornering geometry of the bicycle model [1].

Under steady-state cornering, the lateral force equilibrium can be written as

$$ma_y = F_{yf} + F_{yr}, \tag{2.31}$$

where m is the vehicle mass, a_y is the lateral acceleration, and F_{yf} and F_{yr} are the equivalent front and rear lateral tire forces, respectively.

Moment equilibrium about the center of gravity gives

$$l_f F_{yf} - l_r F_{yr} = 0, \tag{2.32}$$

where l_f and l_r denote the distances from the center of gravity to the front and rear axles.

The lateral acceleration is related to the turning radius by

$$a_y = \frac{v^2}{R}, \tag{2.33}$$

where v is the longitudinal vehicle speed.

Following the steady-state cornering relation in [1], the equivalent steering angle can be written as

$$\delta = \frac{L}{R} + K_u \frac{a_y}{g}, \tag{2.34}$$

where $L = l_f + l_r$ is the wheelbase, g is the gravitational acceleration, and K_u is the understeer gradient. In this thesis, K_u is treated as a calibrated parameter that represents the steady-state understeer characteristic of the vehicle and is used in the equivalent steering-angle relation above.

Substituting (2.33) into (2.34) yields

$$\delta = \frac{L}{v^2} a_y + K_u \frac{a_y}{g}. \tag{2.35}$$

Hence, the lateral acceleration can be expressed as

$$a_y = \frac{\frac{v^2}{L}\delta}{1 + \frac{K_u v^2}{Lg}}. \tag{2.36}$$

Equation (2.36) is used in this thesis to estimate lateral acceleration from vehicle speed and steering input. When $K_u = 0$, the model reduces to the neutral-steer case

$$a_y = \frac{v^2}{L}\delta. \tag{2.37}$$

2.4 Suspension System of the Full-Car Model

The suspension system forms the mechanical interface between the vehicle body and the wheels. Its main functions are to isolate the body from road-induced disturbances in order to improve ride comfort, and to maintain continuous tire contact with the road surface to support handling, stability, and safety [1], [22].

In the full-car model presented in Section 2.2, the suspension is represented by spring, damping, and actuator-force elements acting between the sprung and unsprung masses. These elements provide a simplified dynamic description suitable for control design, while the physical suspension hardware may consist of different practical configurations.

Real vehicles may use different spring and damper layouts, such as coil or air springs together with passive, semi-active, or active dampers. In this thesis, only the suspension configuration relevant to the implemented hydraulic active suspension system is considered.

2.4.1 Passive Spring Element

The passive spring is a mechanical element that stores and releases elastic energy due to the relative vertical displacement between the sprung and unsprung masses. In

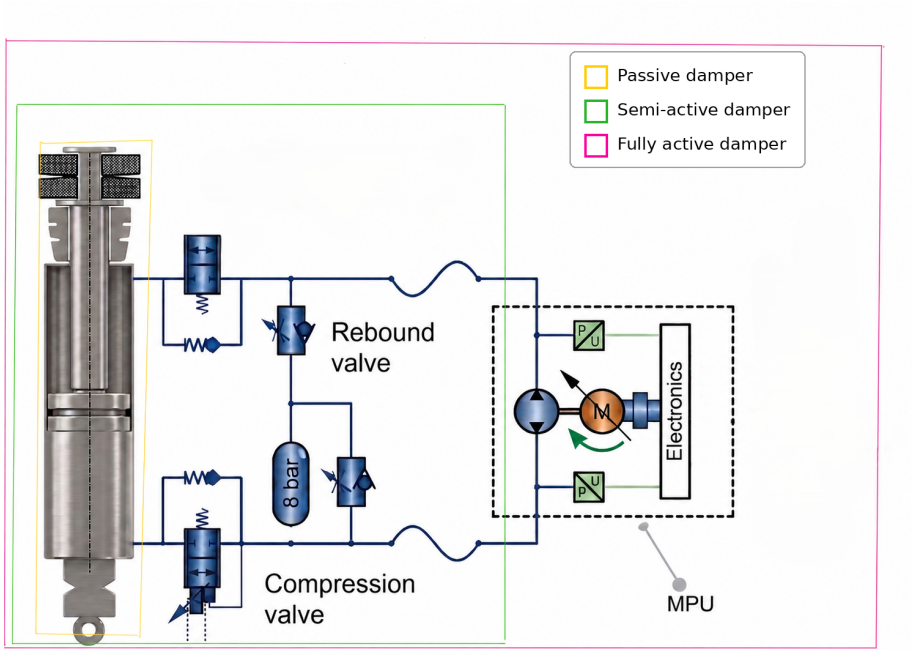

Figure 2.4: Illustration of the hydraulic active damper used in the full-car active suspension system

the full-car model, the spring force is modeled as a linear function of the suspension deflection.

The relative suspension deflection at a suspension corner is defined as

$$\Delta = z_s - z_u, \tag{2.38}$$

where z_s and z_u are the vertical displacements of the sprung and unsprung masses, respectively.

According to Hooke's law, the spring force acting on the sprung mass is written as

$$F_k = -k\Delta = -k(z_s - z_u), \tag{2.39}$$

where F_k is the spring force and k is the spring stiffness. The negative sign indicates that the spring force acts in the direction opposite to the relative suspension deflection.

For the full-car model, different spring stiffness values are used for the front and rear suspension corners. Therefore, the passive spring contribution can be written as

$$F_{k,ij} = -k_{ij}\Delta_{ij}, \tag{2.40}$$

where $ij \in \{fl, fr, rl, rr\}$. Here, $k_{ij} = k_f$ for the front suspension corners and $k_{ij} = k_r$ for the rear suspension corners.

A linear spring model assumes constant stiffness over the considered operating range, as shown in Fig. 2.5. The slope of the force-deflection curve represents the spring stiffness. The origin corresponds to the undeformed or equilibrium condition, where the suspension deflection is zero. With the adopted sign convention, a positive deflection produces a restoring force in the negative direction, while a negative deflection produces a restoring force in the positive direction.

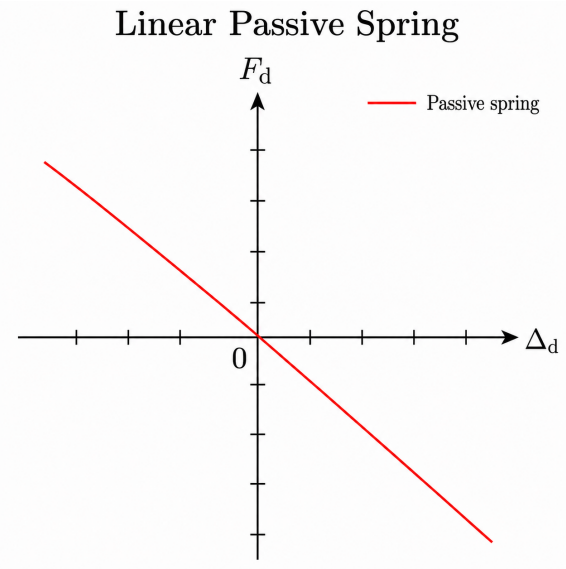

Figure 2.5: Force–Deflection Relationship of a Passive Linear Spring Based on Hooke's Law

2.4.2 Anti-Roll Bar

An anti-roll bar, also called a stabilizer bar, is a passive suspension component that connects the left and right sides of the same axle. During cornering, the outer suspension compresses while the inner suspension extends. This relative motion twists the anti-roll bar and generates a restoring moment that resists vehicle body roll [1], [5].

The anti-roll bar contributes to the total roll stiffness of the vehicle together with the suspension springs. Therefore, it affects the roll angle, roll-gradient response, and lateral load-transfer distribution [1], [22].

2.4.3 Damper

The hydraulic suspension system considered in this thesis is illustrated in Fig. 2.4. It consists of a hydraulic damper, electronically controlled compression and rebound valves, a pressure accumulator, and a motor-pump unit (MPU). Depending on the operating mode, the system can operate in passive, semi-active, or fully active modes.

Throughout this section, the damper deflection velocity is defined as

$$v_d = \dot{z}_s - \dot{z}_u \tag{2.41}$$

where z_s and z_u are the vertical displacements of the sprung and unsprung masses, respectively. Negative v_d denotes compression, while positive v_d denotes rebound. This sign convention is kept the same for passive, semi-active, and fully active operation. What changes between the three cases is the admissible force direction relative to the damper velocity.

2.4.3.1 Passive Suspension

A passive suspension system uses a passive damper whose damping behavior is determined by fixed mechanical components, such as orifices, piston holes, or shim valves. Since these components are not actively controlled, the valve opening remains constant, making the passive damper one of the simplest damper models used in vehicle suspension systems [23].

In the ideal linear model, the damping force is proportional to the relative vertical velocity between the sprung and unsprung masses and always acts opposite to the damper motion. The damping force is therefore written as

$$F_d = -cv_d \tag{2.42}$$

where F_d is the damping force and c is the constant damping coefficient. The negative sign indicates that the passive damper is purely dissipative. Under the adopted sign convention, the passive damping force is positive in compression and negative in rebound.

The passive damper behavior can be represented using linear or nonlinear models, as shown in Fig. 2.6 and Fig. 2.7.

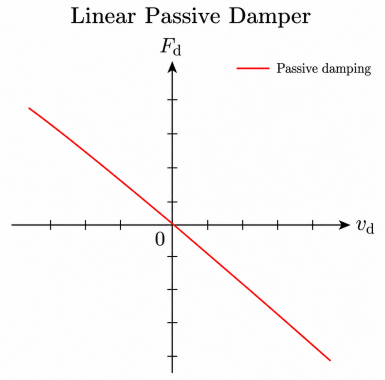

Figure 2.6: Linear passive damper

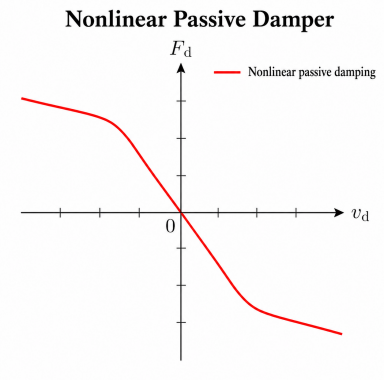

Figure 2.7: Nonlinear passive damper

Although the linear model simplifies the analysis, real passive dampers often show nonlinear behavior. As shown in Fig. 2.7, the damper behaves approximately linearly at low velocities, where the damping force increases almost proportionally with damper velocity. However, beyond a certain velocity, the slope of the force-velocity curve decreases, meaning that the damping force becomes less sensitive to further increases in damper velocity. This behavior appears in both compression and rebound and represents the nonlinear characteristics of practical passive dampers.

The flow sign convention is defined to be consistent with the low-level lookup-table implementation: positive flow for compression and negative flow for rebound.

Due to the piston rod, the effective hydraulic area differs in compression and rebound. To avoid notation overlap with the low-level controller, where A_r denotes piston-rod area, the effective areas in this subsection are denoted A_{comp} and A_{reb}:

$$A_{\text{comp}} = \frac{\pi D_p^2}{4} \tag{2.43}$$

$$A_{\text{reb}} = \frac{\pi}{4}\left(D_p^2 - D_r^2\right) \tag{2.44}$$

where A_{comp} is the compression-side effective area, A_{reb} is the rebound-side effective area, D_p is the piston diameter, and D_r is the piston rod diameter. The damper flow rate can therefore be written as

$$Q_d = \begin{cases} -A_{\text{comp}} v_d, & v_d < 0 \quad \text{compression} \\ 0, & v_d = 0 \\ -A_{\text{reb}} v_d, & v_d > 0 \quad \text{rebound} \end{cases} \tag{2.45}$$

2.4.4 Semi-active Suspension

A semi-active suspension can be considered an extension of a passive suspension system, in which controllable compression and rebound valves are introduced into the damper. These valves allow the damping characteristics to be varied by adjusting the valve openings, as shown inside the green box in Fig. 2.4. This enables the suspension system to adapt to different road and driving conditions more rapidly than a passive suspension.

Unlike a fully active suspension system, a semi-active suspension can only dissipate energy from the system; it cannot inject external energy into the suspension. Therefore, the achievable damper force is limited by the passive nature of the damper and by the physical constraints of the valve system. As in the passive case, the generated force still opposes the damper velocity, although its magnitude can be varied by adjusting the valve openings. The valve command is typically selected based on the damper velocity and the desired damping force. Fig. 2.8 and Fig. 2.9 illustrate simplified linear and nonlinear semi-active damping configurations, respectively.

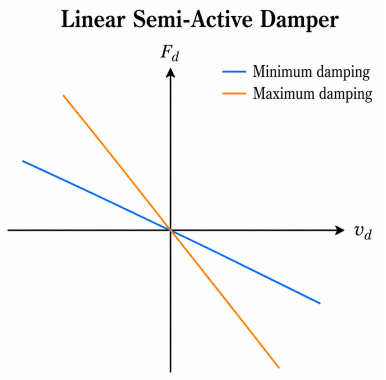

Figure 2.8: Linear semi-active damper

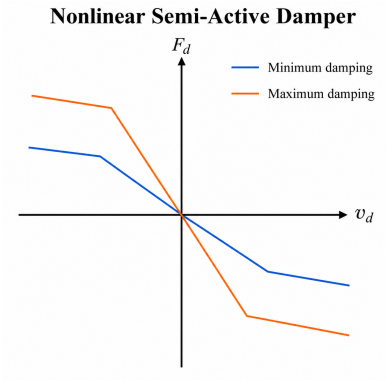

Figure 2.9: Nonlinear semi-active damper

In practice, the damper force may exhibit an approximately linear relationship with the damper deflection velocity at low velocities. At higher velocities, nonlinear valve effects may become significant, causing the force-velocity relationship to deviate from the linear approximation. As in a passive hydraulic damper, piston motion generates hydraulic flow. When this flow passes through the compression or rebound valve, a pressure difference is created, resulting in a damping force.

Therefore, the damping force in a semi-active suspension depends on both the hydraulic flow rate, which is related to the damper velocity, and the valve opening. In this work, the compression and rebound damper forces are represented using black-box nonlinear functions as

$$F_c = f_c(Q_c, u_c), \tag{2.46}$$

$$F_r = f_r(Q_r, u_r), \tag{2.47}$$

where F_c and F_r are the compression and rebound damping forces, respectively. The variables Q_c and Q_r denote the compression and rebound valve flow rates, while u_c and u_r represent the corresponding valve opening commands.

The actual damper force is then selected according to the damper stroke direction:

$$F_d = \begin{cases} F_c, & v_d < 0 \quad \text{compression}, \\ F_r, & v_d \geq 0 \quad \text{rebound}. \end{cases} \tag{2.48}$$

The functions $f_c(\cdot)$ and $f_r(\cdot)$ describe the nonlinear black-box relationships between valve flow rate, valve opening, and generated damping force. With the sign convention adopted above, the semi-active force remains dissipative, with F_c acting in compression and F_r acting in rebound. The compression and rebound valve openings can be adjusted independently. However, they are limited by predefined physical bounds, such that

$$u_{\min} \leq u_c(t) \leq u_{\max} \tag{2.49}$$

$$u_{\min} \leq u_r(t) \leq u_{\max} \tag{2.50}$$

These bounds impose a limitation on the semi-active suspension system. Since the damper can only vary its dissipative characteristics within a finite range, the generated force is constrained between the minimum and maximum achievable damping force characteristics for a given damper velocity. This limitation is illustrated in Fig. 2.8 and Fig. 2.9.

2.4.5 Fully Active Suspension

A fully active suspension can be considered an extension of a semi-active suspension system, in which a motor-pump unit (MPU) is added to the damper. The MPU provides the system with additional capability by allowing energy to be injected into, or dissipated from, the suspension system. Therefore, the force generated by a fully active suspension is not only dependent on the damper deflection velocity, but also on the valve commands and the MPU operation. Unlike passive and semi-active operation, the fully active system is not restricted to generating a force opposite to the damper velocity, since the MPU can supply external energy to the suspension. This wider force-generation capability is illustrated in Fig. 2.4, while the fully active damper structure considered in this work is shown in Fig. 2.10.

The architecture considered in this thesis follows the ZF sMOTION active suspension concept, in which electronically controlled damping is combined with motor–pump-assisted wheel actuation to support body-motion control during driving maneuvers [24].

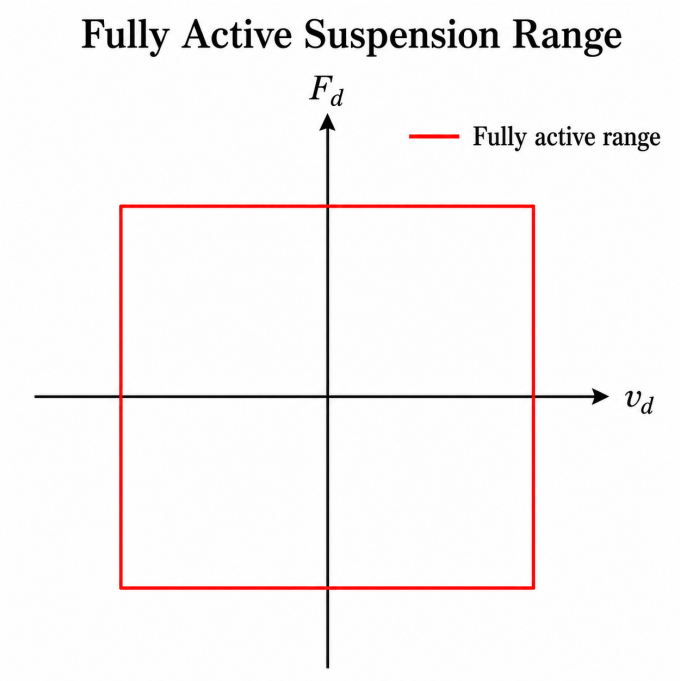

Figure 2.10: Simplified force-generation principle of a fully active suspension damper.

As in the semi-active suspension case, the compression and rebound actions are considered separately. The active suspension force can be written as

$$F_{a,c} = f_{a,c}(v_d, u_c, \mathbf{y}_{\mathrm{MPU}}) \tag{2.51}$$

$$F_{a,r} = f_{a,r}(v_d, u_r, \mathbf{y}_{\mathrm{MPU}}) \tag{2.52}$$

where $F_{a,c}$ and $F_{a,r}$ are the active forces during compression and rebound, respectively. The variable v_d denotes the damper deflection velocity, u_c and u_r are the compression and rebound valve opening commands, and $\mathbf{y}_{\mathrm{MPU}}$ represents the MPU-related input or measured state.

The net active suspension force is selected according to the damper stroke direction:

$$F_a(t) = \begin{cases} F_{a,c}, & v_d < 0 \quad \text{compression}, \\ F_{a,r}, & v_d \geq 0 \quad \text{rebound}. \end{cases} \tag{2.53}$$

Although a fully active suspension can inject energy into the system, the generated force is still limited by the physical actuator and power constraints. Therefore, the active force is bounded as

$$F_{a,\min} \leq F_a(t) \leq F_{a,\max} \tag{2.54}$$

3

Control Theory

This chapter presents the control concepts used in this thesis. It first introduces the hierarchical control architecture used to separate vehicle-level motion control from actuator-level implementation. Feedforward and feedback control are then described as the main strategies for roll, pitch, and heave regulation.

The chapter also introduces PID control as the basis for the implemented PI controllers. Finally, pseudoinverse-based allocation and mode switching control are presented to support the distribution of body-level control demands and the low-level actuator operation.

3.1 Hierarchical Control Architecture

Hierarchical control is commonly used when a complex control problem can be divided into different levels with separate responsibilities. In active suspension systems, this separation is useful because the vehicle-level motion objectives and the actuator-level implementation problem are different in nature. The upper control level is concerned with the desired vehicle dynamic behavior, such as roll, pitch, and heave regulation, while the lower level is responsible for realizing the requested forces using the physical actuator system.

Gáspár and Szabó proposed a hierarchical controller for a full-car active suspension system, where the high-level controller generates a demanded virtual force and the actuator-level controller tracks the reference force by adjusting the actuator valve [25]. This type of structure is advantageous because the high-level controller can be designed based on vehicle-level performance requirements, while the low-level controller can account for actuator nonlinearities, limitations, and force-tracking behavior.

In this thesis, a similar hierarchical idea is adopted. The high-level controller uses vehicle-state information and driver-related inputs to generate desired body-level force and moment demands for roll, pitch, and heave motion. These generalized demands are allocated to the four suspension corners. The low-level controller then converts the requested damper forces into actuator commands, including valve-current commands and motor-pump flow requirements.

A simplified representation of the hierarchical control architecture adopted in this thesis is shown in Fig. 3.1.

This separation improves the modularity of the control design. Changes in the actuator model or valve-control strategy can be handled mainly at the low level, while the high-level body-motion controller can remain largely unchanged.

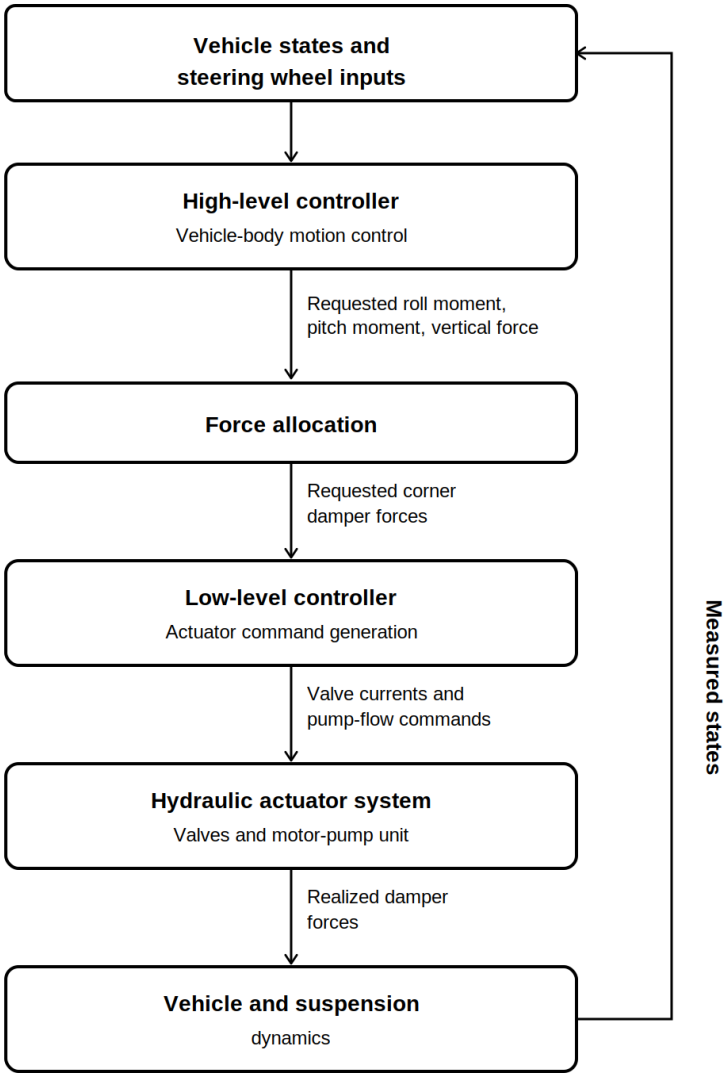

Figure 3.1: Simplified hierarchical control architecture adopted in this thesis.

Similarly, changes in the desired roll-gradient behavior or body-motion objectives can be introduced at the high level without redesigning the complete actuator-control logic.

3.2 Feedforward Control

Feedforward control is a proactive control strategy that counteracts measurable or estimated disturbances before they significantly affect the system response. Unlike feedback control, which reacts after an error has appeared, feedforward control acts in advance based on known input signals or predicted disturbances.

In active suspension systems, an important disturbance is the lateral acceleration generated during cornering. Feedforward and preview-based suspension control methods use measurable or estimated vehicle-motion information to improve the system response before large body-motion errors develop [10], [16]. During cornering, lateral acceleration acting at the height of the vehicle centre of gravity generates an external roll moment about the longitudinal axis. The feedforward controller estimates this disturbance and generates a compensating roll-moment command.

The main advantage of feedforward control is that it can improve the transient response of the suspension system, especially during corner entry. If the disturbance is estimated with sufficient accuracy, the controller can generate a compensating roll-moment command before a large roll-angle error develops. This can reduce the initial roll response and decrease the corrective action required from the feedback controller.

However, the performance of feedforward control depends on the accuracy of the disturbance estimation and the vehicle model. Therefore, feedforward control is usually combined with feedback control to improve robustness and correct remaining roll, pitch, and heave errors.

3.3 Feedback Controller

Feedback control is used to reduce the difference between a desired reference signal and the measured system response. A general feedback control structure is shown in Fig. 3.2. The reference signal $r(t)$ is compared with the measured output $y(t)$, and the difference between them forms the control error

$$e(t) = r(t) - y(t). \tag{3.1}$$

The controller uses this error to calculate the control input $u(t)$, which is applied to the plant. The plant represents the physical system being controlled. The measured output is then fed back to the summation point, forming a closed-loop system [26].

In general, the controller block can represent different types of controllers, such as P, PI, PID, or another control law. The control signal can be written in a general form as

$$u(t) = C(e(t)), \tag{3.2}$$

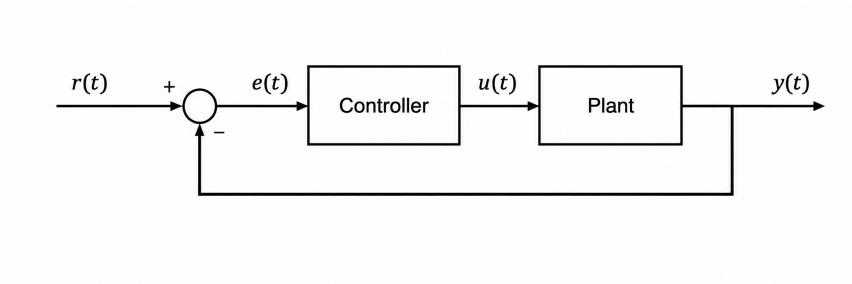

Figure 3.2: General feedback control structure.

3.3.1 PID Controller

A commonly used feedback controller is the proportional–integral–derivative (PID) controller. The PID controller calculates the control input from the control error $e(t)$ using three terms: proportional, integral, and derivative actions. In the time domain, the control law can be written as

$$u(t) = K_p e(t) + K_i \int_0^t e(\tau)\, d\tau + K_d \frac{de(t)}{dt}, \tag{3.3}$$

where K_p, K_i, and K_d are the proportional, integral, and derivative gains, respectively [26]. The proportional term produces a control action directly related to the current error. The integral term depends on the accumulated error over time and is used to reduce steady-state error. The derivative term depends on the rate of change of the error and can improve the transient response by adding damping to the closed-loop system.

The PID controller can therefore be expressed as

$$u(t) = C_{\text{PID}}(e(t)). \tag{3.4}$$

The values of the gains K_p, K_i, and K_d determine the behavior of the controller and must be chosen according to the desired closed-loop response. In general, these gains are not necessarily dimensionless; their units depend on the units of the control error $e(t)$ and the control input $u(t)$.

3.4 Pseudoinverse-Based Allocation

In overactuated control problems, the number of control inputs is larger than the number of generalized control objectives. In such cases, the mapping from the physical input vector to the generalized control vector is not square, and a standard matrix inverse cannot be used directly.

Consider the linear relation

$$y = \mathbf{A}x, \tag{3.5}$$

where $y \in \mathbb{R}^m$ is the generalized control vector, $x \in \mathbb{R}^n$ is the physical input vector, and $\mathbf{A} \in \mathbb{R}^{m \times n}$ is the mapping matrix. When $n > m$, the system is overactuated and infinitely many input vectors may satisfy the same generalized control objective.

A common way to obtain a unique solution is to use the Moore–Penrose pseudoinverse. For a full-row-rank matrix $\mathbf{A}$, the minimum-norm solution is given by

$$x = \mathbf{A}^T \left(\mathbf{A}\mathbf{A}^T\right)^{-1} y. \tag{3.6}$$

This solution satisfies the desired generalized control relation while selecting the input vector with minimum Euclidean norm. In other words, among all feasible solutions, it provides the smallest overall input magnitude.

In this thesis, this pseudoinverse-based allocation method is used to distribute the body-level control demands to the four suspension corners. The allocation input is the generalized control vector $y \in \mathbb{R}^{3\times1}$, and the allocation output is the suspension corner-force vector $x \in \mathbb{R}^{4\times1}$. The corresponding application to the active suspension system is presented in the method chapter.

3.5 Mode Switching Control

Mode switching control is a control approach in which the control action is selected from a finite set of predefined operating modes or controllers. Instead of using a single fixed control law for all operating conditions, a switching rule determines which mode should be active based on the system state, measured signals, or operating conditions.

This concept is closely related to the theory of switched systems. Liberzon and Morse define a switched system as a hybrid dynamical system consisting of a family of continuous-time subsystems and a rule that orchestrates the switching between them [27]. In a control context, these subsystems may represent different controllers, actuator behaviours, or operating modes.

In the low-level control of the fully active suspension system, the valve and actuator operate in different modes depending on the driving condition and the requested damper force from the high-level controller. This allows the actuator behaviour to adapt to different operating conditions while avoiding unnecessary motor-pump activity. In this work, the switching logic is implemented using threshold-based decisions based on steering-wheel velocity, lateral acceleration, requested force, and damper velocity. This provides a structured way to balance roll-control performance, actuator limitations, and energy efficiency.

3.6 Roll and Anti-Roll Motion

When a vehicle enters a corner, lateral acceleration causes load transfer from the inner wheels to the outer wheels. As a result, the outer suspension compresses while the inner suspension extends, and the vehicle body leans toward the outside of the corner. This motion is referred to as body roll.

The roll gradient describes how much the vehicle body rolls for a given lateral acceleration. It is commonly defined as

$$G_\phi = \frac{\phi}{a_y} \quad [\text{deg/g}] \tag{3.7}$$

where ϕ is the body roll angle and a_y is the lateral acceleration.

If the vehicle body instead leans toward the inside of the corner, the motion is referred to as anti-roll motion. In this case, the body roll direction is opposite to the direction associated with conventional cornering-induced roll. In this thesis, different target roll-gradient values are used to produce conventional roll, zero-roll, and anti-roll behaviors.

4

Method

This chapter describes the methodology used to design, implement, and evaluate the proposed hierarchical control strategy for the fully active suspension system. The method consists of a high-level body-motion controller and a low-level actuator controller. The high-level controller generates the desired roll moment, pitch moment, and heave force using feedforward and feedback control. These generalized control demands are then allocated to the four suspension corners and converted into damper-force commands. The low-level controller translates the requested damper forces into actuator commands using lookup tables, mode-switching logic, and pump-flow calculation. Finally, the complete controller is implemented in MATLAB/Simulink and evaluated in IPG CarMaker and the VI-CRT driver-in-the-loop simulator.

4.1 High-Level Control Design

The objective of the high-level controller is to regulate the vehicle body dynamics in terms of roll angle, pitch angle, and heave displacement. The controller generates desired control actions which are then translated into forces applied by the four dampers.

The control architecture consists of a feedforward component that anticipates vehicle motion effects and a feedback component that corrects tracking errors. The resulting moments and forces are then distributed to the four dampers.

The overall control architecture is illustrated in Fig. 4.1.

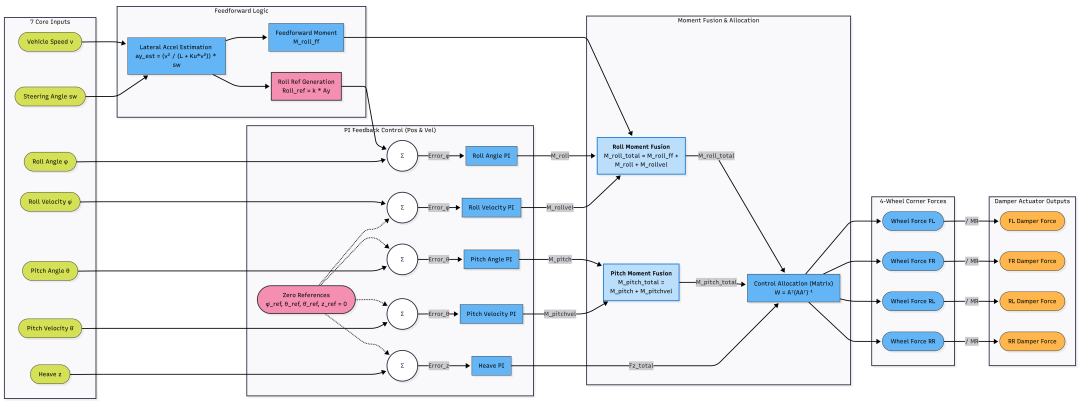

Figure 4.1: High-level control architecture of the active suspension system.

4.1.1 Feedforward Control

The feedforward controller is designed to compensate for predictable disturbances caused by vehicle motion, particularly during cornering.

The inputs to the feedforward controller include:

- Vehicle longitudinal speed (v)
- Steer angle at the front wheels (δ)

4.1.1.1 Lateral Acceleration Estimation

The lateral acceleration (a_y) is estimated using the steady-state bicycle model introduced in Chapter 2. Instead of relying on direct measurements, which may be noisy, a_y is computed from vehicle speed and steering input. If the available steering signal is the steering-wheel angle δ_{sw}, it is first converted into the equivalent front-wheel steering angle δ using the steering ratio relation in Eq.(2.30). The lateral acceleration is then estimated as

$$a_y = \frac{\frac{v^2}{L}\delta}{1 + \frac{K_u v^2}{Lg}} \tag{4.1}$$

where L is the wheelbase, g is the gravitational acceleration, and K_u is the calibrated understeer-gradient parameter introduced in Eq.(2.34).

4.1.1.2 Feedforward Moment Generation

In order to improve the transient response of the control system, a feedforward roll moment is introduced based on the estimated lateral acceleration.

Instead of using a purely proportional formulation, the feedforward term is derived from the balance of roll moments caused by lateral acceleration. According to [10], the roll moment induced by lateral acceleration can be expressed as:

$$M_x = \left[m_s h_{CMC} + 2\left(m_{wf} R_{wh_f} + m_{wr} R_{wh_r}\right)\right] a_y \tag{4.2}$$

where:

- m_s is the sprung mass
- h_{CMC} is the height of the center of mass of the chassis above the ground
- m_{wf} and m_{wr} are the unsprung front and rear masses.
- R_{wh_f} and R_{wh_r} are the radius of the front and rear wheels, respectively

Based on this relation, the feedforward roll moment is directly computed as:

$$M_\phi^{ff} = M_x \tag{4.3}$$

This formulation allows the controller to directly compensate for the roll moment induced by lateral acceleration. As a result, the feedforward action anticipates load transfer and reduces the burden on the feedback controller, leading to improved transient performance.

4.1.2 Feedback Control (PI)

The feedback controller regulates the system states:

- Roll angle (ϕ)
- Roll rate ($\dot{\phi}$)
- Pitch angle (θ)
- Pitch rate ($\dot{\theta}$)
- Heave displacement (z)

The control structure is composed of both angle and rate feedback loops. The angle-based PI controllers are primarily used to regulate the vehicle body posture, ensuring that the roll and pitch angles track their desired references.

In addition, the rate-based PI controllers, using roll rate ($\dot{\phi}$) and pitch rate ($\dot{\theta}$), provide a damping effect to the system. This can be interpreted as a form of virtual damping, which helps to suppress oscillations and improve transient response.

In industrial applications, derivative (D) terms are often avoided due to their sensitivity to measurement noise and implementation challenges. Therefore, instead of directly using a D term, the rate signals are explicitly measured and controlled through PI loops, achieving a similar damping effect in a more robust and practical manner. The primary control objective is defined in terms of the desired roll gradient. Based on this, the reference roll angle is constructed as a function of the lateral acceleration:

$$\phi_{ref} = \frac{\pi}{180} G_\phi \frac{a_y}{g} \tag{4.4}$$

where G_ϕ is the desired roll gradient. For the remaining states, the reference values are set to zero:

$$\theta_{ref} = 0, \quad \dot{\phi}_{ref} = 0, \quad \dot{\theta}_{ref} = 0, \quad z_{ref} = 0 \tag{4.5}$$

4.1.2.1 Roll Control

The roll angle control error is defined as:

$$e_\phi = \phi_{ref} - \phi \tag{4.6}$$

The roll moment is generated using a PI controller:

$$M_\phi = K_{p\phi} e_\phi + K_{i\phi} \int e_\phi \, dt \tag{4.7}$$

Additionally, the roll rate is regulated to improve damping:

$$e_{\dot{\phi}} = \dot{\phi}_{ref} - \dot{\phi} \tag{4.8}$$

$$M_{\dot{\phi}} = K_{p\dot{\phi}} e_{\dot{\phi}} + K_{i\dot{\phi}} \int e_{\dot{\phi}}\, dt \tag{4.9}$$

4.1.2.2 Pitch Control

The pitch angle error is defined as:

$$e_\theta = \theta_{ref} - \theta \tag{4.10}$$

$$M_\theta = K_{p\theta} e_\theta + K_{i\theta} \int e_\theta\, dt \tag{4.11}$$

Similarly, the pitch rate is controlled as:

$$e_{\dot{\theta}} = \dot{\theta}_{ref} - \dot{\theta} \tag{4.12}$$

$$M_{\dot{\theta}} = K_{p\dot{\theta}} e_{\dot{\theta}} + K_{i\dot{\theta}} \int e_{\dot{\theta}}\, dt \tag{4.13}$$

4.1.2.3 Heave Control

The heave control error is defined as:

$$e_z = z_{ref} - z \tag{4.14}$$

$$F_z = K_{pz} e_z + K_{iz} \int e_z\, dt \tag{4.15}$$

4.1.3 Control Combination

The total desired control actions are obtained by combining feedforward and feedback terms.

For the roll dynamics, both angle and rate feedback contributions are included together with the feedforward term:

$$M_\phi^{tot} = M_\phi + M_{\dot{\phi}} + M_\phi^{ff} \tag{4.16}$$

For the pitch dynamics, both angle and rate feedback are combined:

$$M_\theta^{tot} = M_\theta + M_{\dot{\theta}} \tag{4.17}$$

For the vertical (heave) dynamics, the total force is obtained from the PI controller:

$$F_z^{tot} = F_z \tag{4.18}$$

4.1.4 Force Allocation Strategy

The pseudoinverse-based allocation method introduced in the control theory chapter is used here to distribute the body-level control actions to the four suspension corners. After combining the feedforward and feedback terms, the generalized control vector is written as

$$u_g(t) = \begin{bmatrix} F_z^{tot} & M_\phi^{tot} & M_\theta^{tot} \end{bmatrix}^T, \tag{4.19}$$

where F_z^{tot} is the total heave control force, M_ϕ^{tot} is the total roll control moment, and M_θ^{tot} is the total pitch control moment.

The corresponding corner-force vector is written as

$$\mathbf{f}_c(t) = \begin{bmatrix} f_{fl}(t) & f_{fr}(t) & f_{rl}(t) & f_{rr}(t) \end{bmatrix}^T, \tag{4.20}$$

where f_{fl}, f_{fr}, f_{rl}, and f_{rr} denote the controllable suspension corner forces at the four corners.

Using the vehicle geometry, the mapping between generalized control inputs and corner forces is expressed as

$$u_g(t) = \mathbf{A}\mathbf{f}_c(t), \tag{4.21}$$

with

$$\mathbf{A} = \begin{bmatrix} 1 & 1 & 1 & 1 \\ t_l & -t_r & t_l & -t_r \\ -l_f & -l_f & l_r & l_r \end{bmatrix}. \tag{4.22}$$

Because the system has four corner forces but only three generalized control targets, the allocation problem is overactuated. In the implementation, the corner-force vector is obtained using the minimum-norm pseudoinverse solution

$$\mathbf{f}_c(t) = \mathbf{A}^\dagger u_g(t), \tag{4.23}$$

where

$$\mathbf{A}^\dagger = \mathbf{A}^T \left(\mathbf{A}\mathbf{A}^T\right)^{-1}. \tag{4.24}$$

Thus, the implemented allocation law can be written as

$$\begin{bmatrix} f_{fl}(t) \\ f_{fr}(t) \\ f_{rl}(t) \\ f_{rr}(t) \end{bmatrix} = \mathbf{A}^\dagger \begin{bmatrix} F_z^{tot} \\ M_\phi^{tot} \\ M_\theta^{tot} \end{bmatrix}. \tag{4.25}$$

This mapping is identical to the source-code implementation and distributes the total heave, roll, and pitch control actions to the four suspension corners according to the vehicle geometry.

4.1.5 Motion Ratio Conversion

The allocated corner forces f_{fl}, f_{fr}, f_{rl}, and f_{rr} represent the controllable suspension corner forces in the full-car model. However, the low-level controller acts on

the damper actuator. Therefore, these corner forces must be converted into the corresponding damper-side forces through the suspension motion ratio.

The motion ratio, denoted by MR, is defined as the local kinematic ratio between damper stroke and wheel vertical displacement:

$$MR = \frac{\Delta z_{\text{damper}}}{\Delta z_{\text{wheel}}}, \tag{4.26}$$

where Δz_{damper} is the change in damper displacement and Δz_{wheel} is the corresponding vertical displacement of the wheel center. In this thesis, separate constant motion-ratio values are used for the front and rear axles and are denoted by MR_{front} and MR_{rear}, respectively.

The motion-ratio values were obtained from a pre-run of the suspension kinematics. In this pre-run, the wheel center was moved vertically around the nominal static ride height, and the corresponding damper displacement was recorded. The motion ratio was then calculated from the local slope between damper displacement and wheel vertical displacement. Only the geometric suspension kinematics were considered in this calculation; compliance effects from bushings, mounts, and other elastic components were not included.

Based on virtual work, the wheel-side suspension force and the damper-side force satisfy

$$f_{ij}\Delta z_{\text{wheel}} = F^{\text{req}}_{\text{damper}}\Delta z_{\text{damper}}. \tag{4.27}$$

Therefore, the required damper force is obtained as

$$F^{\text{req}}_{\text{damper}} = \frac{f_{ij}}{MR}, \tag{4.28}$$

where f_{ij} denotes the allocated controllable suspension corner force and $F^{\text{req}}_{\text{damper}}$ is the corresponding damper-side force.

4.2 Low-Level Control

The low-level controller is responsible for translating the desired suspension forces into actuator-level commands. Specifically, it converts the required damper forces into CCD current commands and MPU flow-rate commands.

In this work, the control structure is simplified into two main components. First, a mode switching logic determines the actuator operating state and generates the corresponding current commands for compression and rebound. This decision is based on the requested force and key system states, including lateral acceleration, steering velocity, and damper velocity.

Second, based on the selected operating mode, the required valve flow is determined and used to compute the corresponding motor pump flow. The pump flow is calculated as the difference between the required valve flow and the flow induced by the damper motion.

The overall structure of the low-level controller is illustrated in Fig. 4.2.

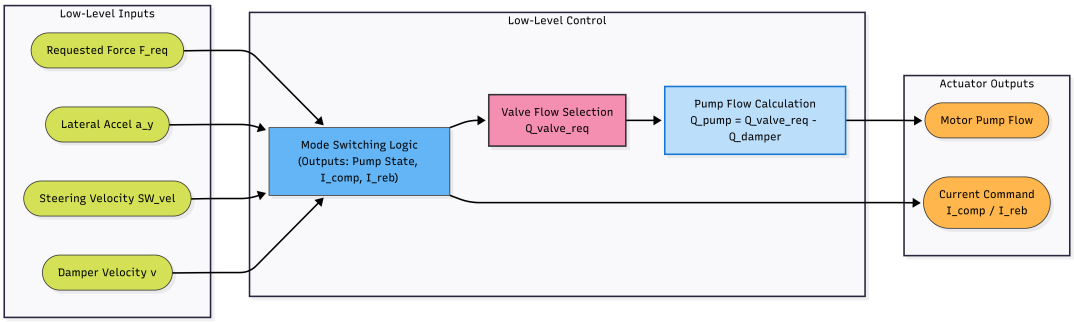

Figure 4.2: Simplified low-level control structure. The mode switching logic determines the actuator state and current commands, while the valve flow selection and pump flow calculation generate the required motor pump flow.

As shown in Fig. 4.2, the control logic is organized into a mode-based decision block and a flow-based computation block. This structure allows a clear separation between decision-making and physical actuation, enabling efficient and robust implementation of the low-level controller.

4.2.1 Motor–Pump Modeling Using Lookup Tables

In the low-level control, the actuator behavior is modeled using lookup tables derived from supplier data. This approach allows capturing the nonlinear relationship between damper force, current, and hydraulic flow without relying on simplified analytical models.

The actuator is characterized by a nonlinear mapping between the generated force, current, and hydraulic flow, which can be expressed as:

$$F = f(Q, I) \tag{4.29}$$

where F is the damper force, Q is the hydraulic flow, and I is the current.

In practice, the hydraulic flow is obtained from the damper velocity through piston geometry. Due to the piston rod, different effective piston areas are used for rebound and compression. The valve flow is calculated as:

$$Q = \begin{cases} -v_d \left(A_p - A_r\right), & v_d \geq 0 \quad \text{(rebound)} \\ -v_d A_p, & v_d < 0 \quad \text{(compression)} \end{cases} \tag{4.30}$$

where Q is the valve flow, v_d is the damper velocity, A_p is the piston area, and A_r is the piston rod area. When $v_d \geq 0$, the damper is in rebound and the rod-side effective area is used. When $v_d < 0$, the damper is in compression and the full piston area is used.

This area difference results in asymmetric actuator behavior between rebound and compression, which is explicitly considered in the lookup table construction.

Based on this relationship, an inverse mapping is constructed for control implementation, allowing the required current to be determined from the desired force:

$$I = f(F, Q) \tag{4.31}$$

In addition, an auxiliary mapping is constructed to estimate the hydraulic flow from force and current:

$$Q = f(F, I) \tag{4.32}$$

It should be noted that the sign convention used in the lookup tables is consistent with the physical damper model introduced earlier in this thesis. The flow is defined based on damper motion, where negative flow represents rebound and positive flow represents compression. The damper force is defined using the same convention, with positive values associated with compression and negative values associated with rebound. This convention is applied consistently throughout the low-level controller.

The lookup tables used in this work are obtained from supplier-provided data and further processed to improve numerical properties. In particular, a non-uniform discretization is applied to the flow axis, providing higher resolution near zero flow to enhance interpolation accuracy in low-velocity regions. In addition, smoothing techniques are applied to the inverse lookup table to remove discontinuities and ensure stable behavior in real-time implementation.

Fig. 4.3a illustrates the forward mapping between force, flow, and current. Fig. 4.3b shows the inverse mapping used in the controller to compute the required current for a given force demand. Fig. 4.3c shows the auxiliary flow mapping from force and current.

This lookup-table-based modeling approach enables an accurate representation of the actuator characteristics while maintaining computational efficiency, making it suitable for real-time control implementation.

4.2.2 Mode Switching Logic for Low-Level Control

In addition to the actuator mapping, a mode switching strategy is introduced in the low-level controller to determine how the motor–pump system should operate under different driving conditions. The logic is designed to balance performance, energy efficiency, and actuator limitations.

The overall decision process is illustrated in Fig. 4.4. The control logic evaluates the driving condition and the requested force, and then selects an appropriate operating mode.

4.2.2.1 Driving Condition Identification

The first step is to identify aggressive steering behavior, which is commonly used in advanced damper control strategies to distinguish dynamic driving conditions [28]. A speed-dependent steering-velocity threshold is used:

$$\left|\dot{\delta}\right| > \dot{\delta}_{th}(v). \tag{4.33}$$

When this condition is satisfied, the system enters a predictive hard mode (Mode 1), providing high support to improve vehicle stability during rapid maneuvers.

If no high steering activity is detected, the lateral acceleration a_y is used to determine whether the vehicle is driving in a straight line. When

$$|a_y| < a_{y,th}, \tag{4.34}$$

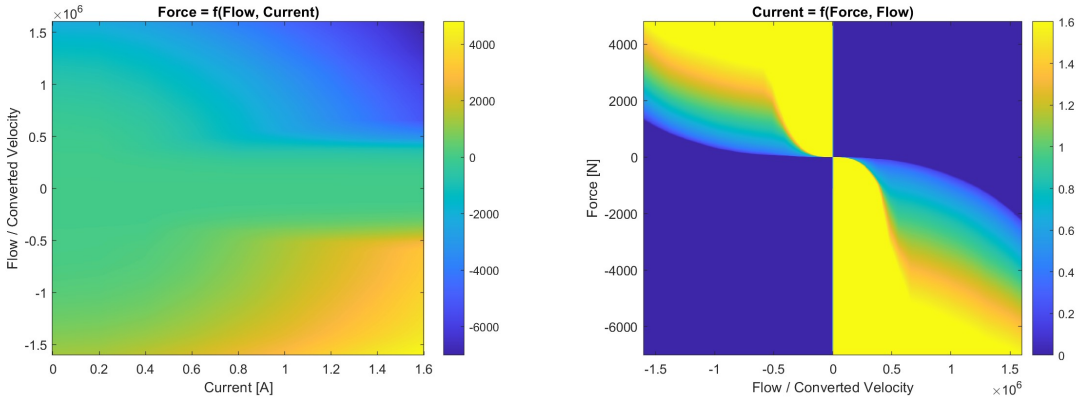

(a) $F = f(Q, I)$ **(b)** $I = f(F, Q)$

(c) $Q = f(F, I)$

Figure 4.3: Lookup-table-based actuator mappings.

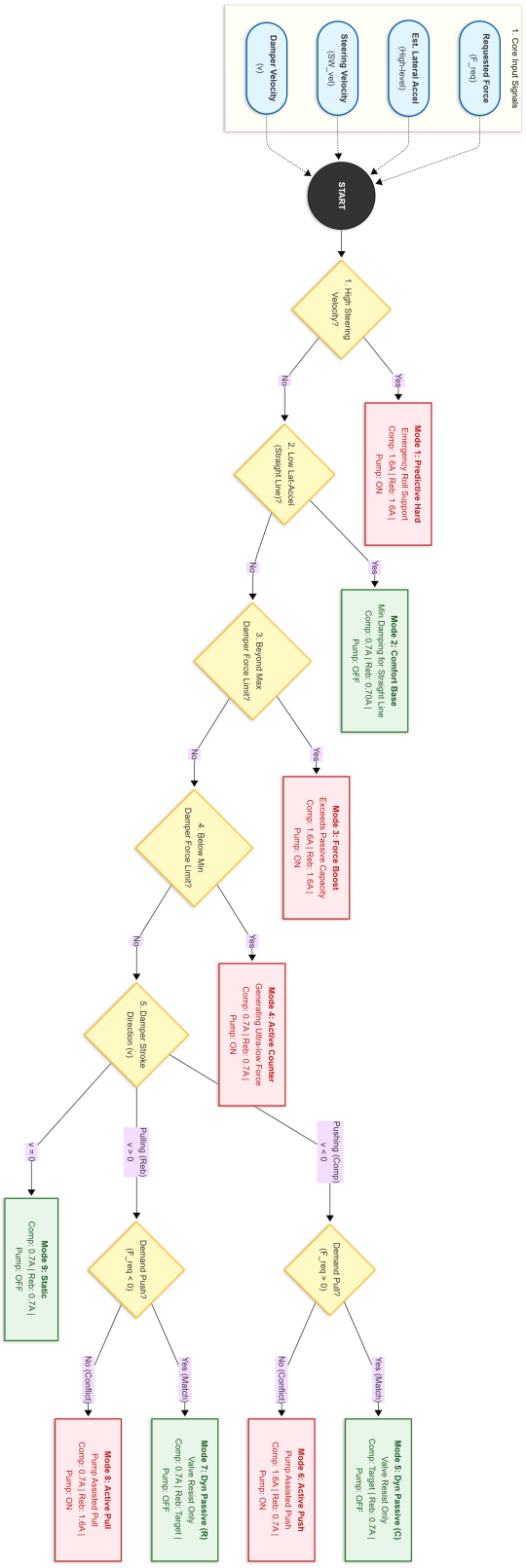

Figure 4.4: Mode switching logic for the low-level actuator control.

the system operates in a comfort-oriented passive mode (Mode 2), where minimal damping is applied and the pump is turned off to reduce energy consumption.

4.2.2.2 Force-Based Mode Selection

If the vehicle is not in a straight-line condition, the requested force F_{req} is evaluated with respect to actuator capability. When

$$F_{req} > F_{\max}(Q), \tag{4.35}$$

a force boost mode (Mode 3) is activated, where the motor–pump system provides additional force beyond passive capability.

Similarly, when

$$F_{req} < F_{\min}(Q), \tag{4.36}$$

an active counter mode (Mode 4) is selected to generate small or counteracting forces.

4.2.2.3 Stroke Direction and Actuation Modes

For intermediate force levels, the actuator behavior depends on the damper stroke direction, which is determined by the damper velocity. Two directions are distinguished:

- Compression ($v_d < 0$)
- Rebound ($v_d > 0$)

Based on the stroke direction and the sign of the requested force, the controller determines whether the demanded force aligns with the natural damping force. If the force direction matches the passive damping behavior, the system operates in a dynamic passive mode (Mode 5 or Mode 7), where only valve resistance is used and the pump remains off.

Otherwise, active assistance is required. In this case, pump-assisted modes are activated, including active push (Mode 6) and active pull (Mode 8), depending on the force direction and stroke condition.

In addition, when

$$|v_d| < v_{d,th}, \tag{4.37}$$

the system switches to a static mode (Mode 9). In this mode, no active pumping is performed and the actuator remains inactive, as the required force can be maintained with minimal or zero flow. This threshold-based switching strategy improves energy efficiency by avoiding unnecessary actuation under near-zero motion conditions.

4.2.2.4 Derived Variables and Parameter Settings

The key variables used in the mode switching logic are derived from the lookup-table-based actuator model:

- The dynamic target current I is obtained from the inverse lookup table:

$$I = f(F_{req}, Q)$$

- The passive force limits $F_{\max}$ and $F_{\min}$ are obtained from the forward lookup table:

$$F = f(Q, I)$$

4.2.2.5 Independent Compression and Rebound Current Control

To accurately realize the desired force, separate current commands are introduced for compression and rebound:

- Compression current (I_{comp})
- Rebound current (I_{reb})

This separation allows the controller to account for the asymmetric behavior of the actuator and to independently regulate force generation in compression and rebound phases. It also provides greater flexibility in mode switching, especially during transitions between passive and active operation.

4.2.2.6 Summary

The proposed mode switching strategy ensures that the actuator operates in the most appropriate mode under varying conditions. By combining condition-based switching with force limits and stroke direction analysis, the controller achieves a balance between performance, robustness, and energy efficiency.

4.2.3 Pump Flow Calculation

After the operating mode is selected, the required pump flow is calculated based on the valve flow demand. The requested valve flow is obtained from the lookup table using the requested force and the maximum current level of 1.6 A:

$$Q_{req} = f(F_{req}, I_{max}) \tag{4.38}$$

where Q_{req} is the requested valve flow, F_{req} is the required damper force, and $I_{max} = 1.6$ A is the maximum actuator current.

The final required valve flow depends on whether the motor–pump system is activated. If the motor–pump is not active, the controller uses the passive damper valve flow. If the motor–pump is active, the controller uses the requested active valve flow:

$$Q_{valve}^{req} = \begin{cases} Q_{damper}, & \text{if motor–pump is OFF} \\ Q_{req}, & \text{if motor–pump is ON} \end{cases} \tag{4.39}$$

where Q_{damper} is the valve flow generated by the damper motion.

The required pump flow is then calculated as the difference between the required valve flow and the actual damper valve flow:

$$Q_{pump}^{req} = Q_{valve}^{req} - Q_{damper} \tag{4.40}$$

This calculation ensures that the motor–pump system only provides the additional flow needed to achieve the requested actuator behavior. When the motor–pump is off, the required pump flow becomes zero, and the actuator behaves as a passive or semi-active damper.

4.3 Implementation of the Method

This section explains how the proposed control strategy is implemented in simulation and clarifies the key calibration and scenario parameters used in this thesis.

4.3.1 Controller Execution Pipeline

At each control step, the controller is executed in the following sequence:

1. Estimate lateral acceleration from vehicle speed and steering input using (4.1).
2. Compute high-level generalized control targets (f_z, f_θ, f_ϕ) by combining feedforward and feedback terms.
3. Convert generalized targets into corner actuator forces via the input decoupling transformation matrix (4.24).
4. Convert wheel-level force demands to damper-level force demands using motion-ratio conversion.
5. Execute low-level mode switching and lookup-table mapping to generate current and flow commands.
6. Apply the resulting corner suspension forces to the vehicle model through the external suspension-force interface.

The same control structure is used for both CarMaker and VI-CRT validation. After calibration, controller gains and switching thresholds are kept fixed across all reported test cases.

4.3.2 CarMaker Simulation

4.3.2.1 Scenario and Maneuver

The simulation scenario is designed to evaluate the roll motion control performance under a representative cornering maneuver. The road layout used in the simulation is illustrated in Fig. 4.5.

The vehicle initially travels in a straight line at a constant speed of 16 km/h for a distance of 100 m. After that, the vehicle enters a circular path with a radius

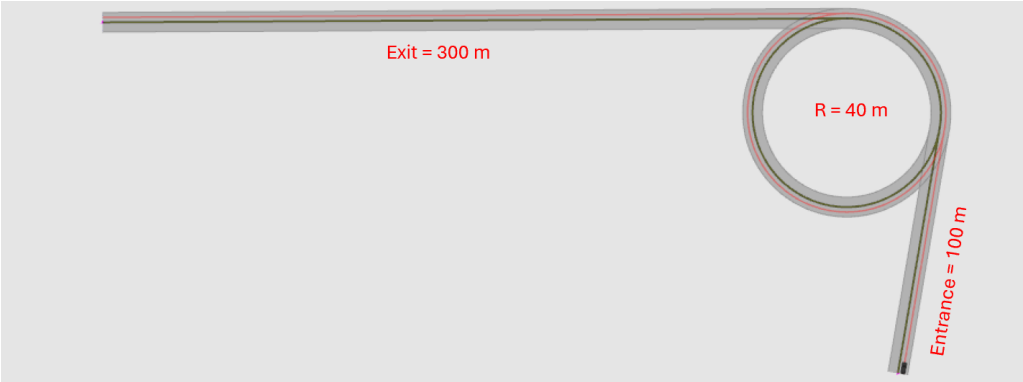

Figure 4.5: Driving scenario used in CarMaker simulation.

of 40 m. During the cornering phase, the lateral acceleration is increased gradually, with a lateral jerk limited to 0.01 g/s, in order to ensure a smooth transition. The vehicle continues accelerating until the lateral acceleration reaches 0.8 g. After reaching the peak lateral acceleration, the vehicle exits the corner and returns to straight-line driving for an additional distance of 300 m, while maintaining the same vehicle speed as at the end of the cornering phase.

This maneuver allows evaluation of both transient and steady-state roll behavior.

Table 4.1 summarizes the key parameters disclosed in this work.

Table 4.1: Key calibration and scenario parameters used in this thesis.

Parameter	Value	Description
G_ϕ	+4 deg/g, 0 deg/g, −4 deg/g	Roll-gradient targets used in evaluation
$I_{\max}$	1.6 A	Maximum actuator current in low-level controller
v_{init}	16 km/h	Initial straight-line speed in CarMaker maneuver
R_{turn}	40 m	Radius of constant-curvature corner
$\dot{a}_{y,\max}$	0.01 g/s	Lateral-jerk limit during corner entry
$a_{y,\max}$	0.8 g	Peak lateral acceleration target
d_{in}	100 m	Pre-corner straight-line distance
d_{out}	300 m	Post-corner straight-line distance

Vehicle geometric and mass-related parameters (l_f, l_r, t_l, t_r, m_s, m_{wf}, m_{wr}, h_{CMC}, R_{wh_f}, R_{wh_r}, A_p, A_r, MR_{front}, MR_{rear}) are taken from the validated vehicle model configuration. PI gains and switching thresholds are tuned offline and then fixed during all experiments.

4.3.2.2 Simulink Integration with CarMaker

In order to evaluate the proposed control strategy in a realistic simulation environment, CarMaker is coupled with Simulink to implement the active suspension control system.

In the CarMaker vehicle model, the original suspension components, including the passive damper and anti-roll bar, are disabled. Instead, the suspension forces

are fully controlled by an external control model implemented in Simulink. This approach allows the active suspension controller to directly generate the required forces at each wheel.

Specifically, the control model outputs the suspension forces for the four corners of the vehicle, namely front-left (FL), front-right (FR), rear-left (RL), and rear-right (RR). These forces are provided to CarMaker through the interface *External Suspension Forces*, replacing the internal suspension forces of the default vehicle model.

The overall control structure is illustrated in Fig. 4.6. The block *Active Suspension Control* represents the implemented high-level and low-level controllers, which compute the required damper forces based on vehicle states. These forces are then sent to CarMaker as external inputs, ensuring that the vehicle dynamics are governed by the designed control strategy.

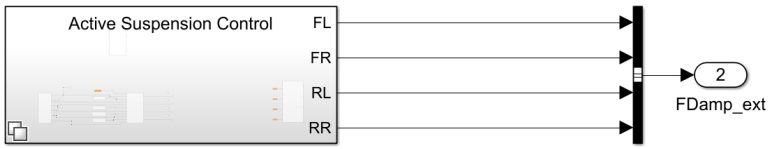

Figure 4.6: Simulink–CarMaker integration for active suspension control. The controller outputs suspension forces (FL, FR, RL, RR), which are applied to the vehicle model via the External Suspension Forces interface.

4.3.3 VI-CRT Simulator

To further validate the proposed active suspension control strategy in a more realistic environment, the system is implemented and tested in the VI-CRT simulator, based on the VI-CarRealTime real-time vehicle simulation environment from VI-grade [29], [30]. Compared to the CarMaker simulation, the VI-CRT platform provides a real-time simulation environment with driver-in-the-loop capability. This allows evaluation of the control system under more realistic operating conditions, including real-time execution constraints, human driver inputs, and varying driving behaviors.

4.3.3.1 Control-System Integration

The Simulink model developed for the CarMaker simulation is reused in the VI-CRT environment without changes to the control structure. The active suspension control system, including both high-level and low-level controllers, continues to generate the required suspension forces, which are applied to the vehicle model through the external suspension force interface.

Unlike the predefined maneuver used in the CarMaker simulation, no fixed driving scenario is imposed in the VI-CRT simulator. Instead, the vehicle is driven manually by a human driver, resulting in varying steering inputs and dynamic conditions. This setup enables evaluation of the robustness and adaptability of the

proposed control strategy under more realistic and less predictable driving conditions.

A simplified and redrawn overview of the Simulink–VI-CRT integration is shown in Fig. 4.7. The overview highlights the VI-CarRealTime vehicle model, the active-suspension controller subsystem, the main signal routing, and selected signal-processing blocks used for the real-time implementation.

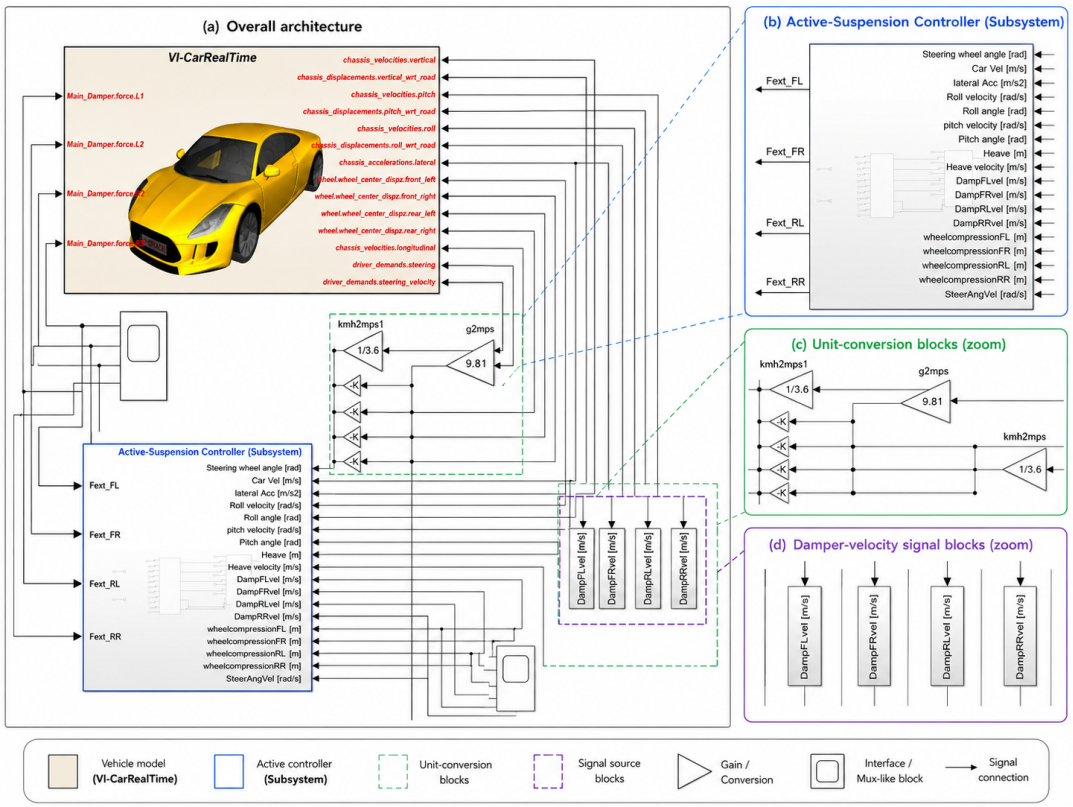

Figure 4.7: Redrawn overview of the Simulink model integrated with the VI-CRT simulator for real-time validation of the active suspension control system. The figure shows the VI-CarRealTime vehicle model, the active-suspension controller subsystem, the main signal routing, and enlarged views of the controller inputs, unit-conversion blocks, and damper-velocity signal blocks. The VI-CarRealTime/VI-CRT block is part of the VI-grade real-time simulation toolchain [29], [30].

4.3.3.2 Driver-in-the-Loop Setup

In addition to the control-system integration shown in Fig. 4.7, the VI-CRT platform provides a driver-in-the-loop simulation environment in which a human driver interacts with the virtual vehicle in real time. The driver applies steering, throttle, and braking inputs through the simulator hardware while receiving visual feedback from the simulated driving scene. This setup makes it possible to evaluate the proposed active suspension control strategy under closed-loop driving conditions that include human input variability and real-time simulator interaction.

The physical driver-in-the-loop simulator environment used in this work is shown in Fig. 4.8.

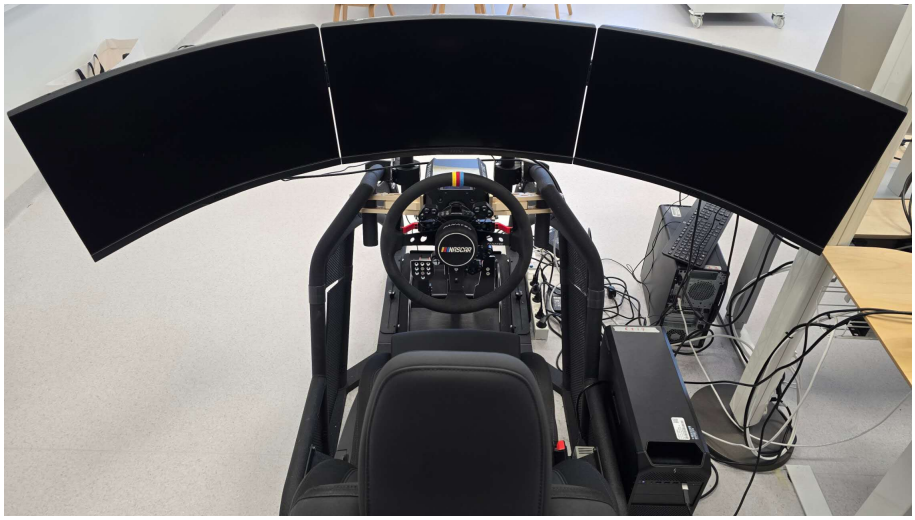

Figure 4.8: Driver-in-the-loop setup of the VI-CRT simulator used for real-time evaluation.

5

Results

This chapter presents the results used to evaluate the proposed roll-motion control strategy for the fully active suspension system. The controller is first assessed in IPG CarMaker using one passive baseline case and three active roll-gradient targets: positive, zero, and negative roll. The passive baseline includes the passive dampers and anti-roll bar, whereas the fully active cases remove the anti-roll bar and use vertical actuator forces to control the roll response. The analysis focuses on roll-angle response, suspension-force distribution, and actuator force tracking.

The controller is then evaluated in the VI-CRT driver-in-the-loop simulator to examine whether the desired roll behaviour is maintained under real-time driving conditions. The same suspension configurations are used in the VI-CRT evaluation: the passive reference includes the anti-roll bar, while the fully active cases remove it and use vertical actuator forces to control the roll response.

5.1 CarMaker Simulation Results

Before evaluating the roll-gradient responses, the main vehicle input signals for the common CarMaker scenario are shown in Figure 5.1. The same scenario is used for the passive reference and for all active roll-gradient cases, which allows the different suspension-control settings to be compared under the same driving conditions. The steering input defines the cornering manoeuvre, while the longitudinal velocity and lateral acceleration describe the operating conditions during the test. The velocity is presented in km/h for readability, and the lateral acceleration is shown in g to be consistent with the roll-gradient unit used in this thesis.

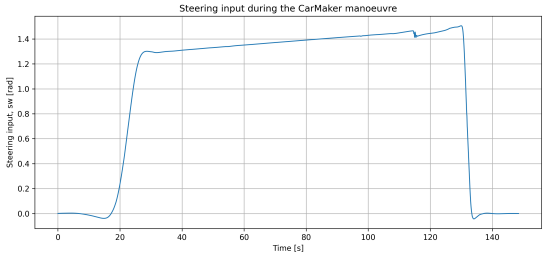

(a) Steering input, sw [rad].

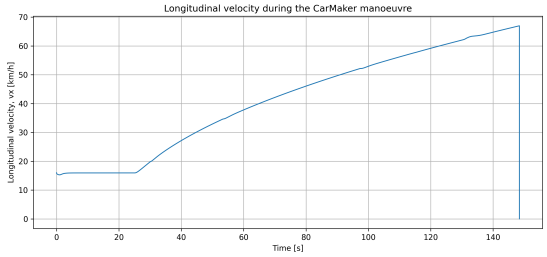

(b) Longitudinal velocity, v_x [km/h].

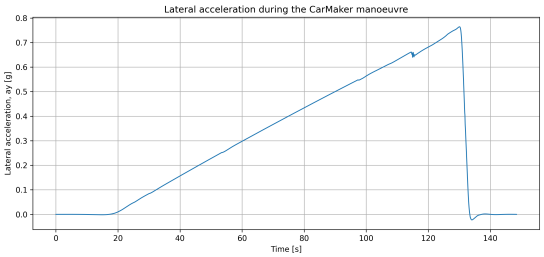

(c) Lateral acceleration, a_y [g].

Figure 5.1: Input signals for the common CarMaker scenario used for the passive reference and active roll-gradient cases.

5.1.1 Passive Damper Baseline with Anti-Roll Bar

Before evaluating the active suspension controller, a passive reference case is simulated in CarMaker using the passive dampers together with the anti-roll bar. This case provides a baseline for the natural roll response of the vehicle when no active suspension force is applied. In the fully active suspension cases, the anti-roll bar is removed, and the roll response is controlled by vertical actuator forces at the suspension corners.

Figure 5.2 shows the roll angle as a function of lateral acceleration for the passive configuration used as the simulation baseline. After a small transient variation around zero lateral acceleration, the roll angle increases almost linearly as lateral acceleration builds up during cornering, which is the expected behavior for a conventional suspension system. In this baseline configuration, the passive response is slightly steeper than the 4 deg/g reference line. At 0.7 g, the passive simulation data give a roll angle of 3.06 deg, while the 4 deg/g reference corresponds to 2.80 deg at the same lateral acceleration.

This result should not be interpreted as showing that a passive suspension cannot be tuned to meet a single roll-gradient requirement. The roll gradient of a passive vehicle could be changed by modifying the spring stiffness, damper characteristics, or anti-roll-bar stiffness. However, once these passive parameters are selected, the response is fixed by the mechanical design and cannot be adjusted during operation to follow different prescribed roll-gradient targets. The passive baseline therefore serves as a fixed mechanical reference, while the active suspension cases presented in the following sections use controllable suspension forces to track positive, zero, and negative roll-gradient targets with the same control structure.

The roll-gradient responses are also evaluated quantitatively in order to com-

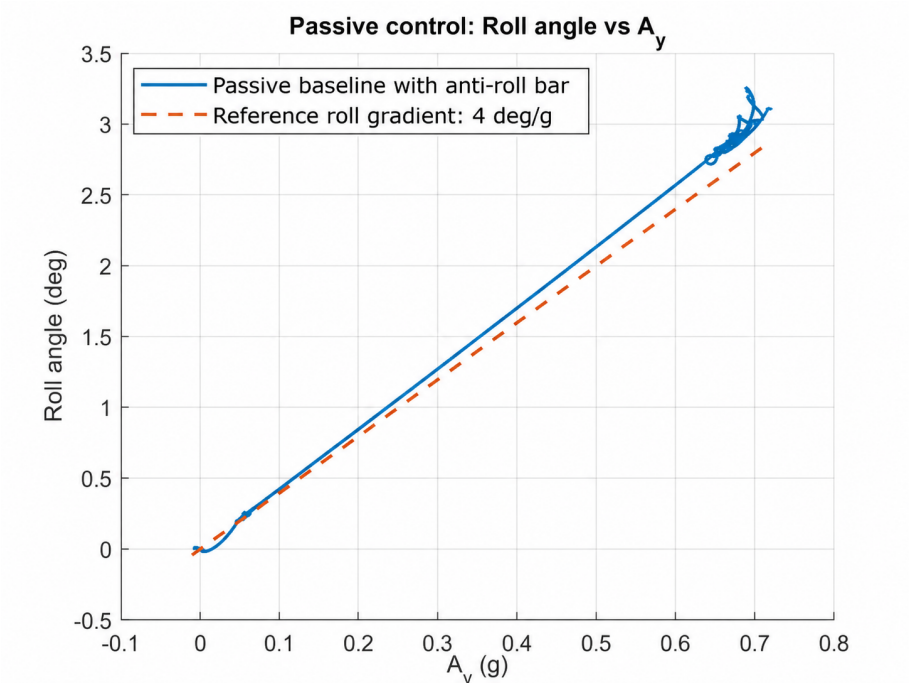

Figure 5.2: Passive damper baseline with anti-roll bar: roll angle as a function of lateral acceleration.

pare the passive baseline and the active-control cases. The fitted roll gradient is obtained by applying a least-squares linear fit between roll angle ϕ and lateral acceleration a_y. The roll angle at 0.7 g is obtained from the simulation data at the sample closest to 0.7 g. The maximum absolute roll angle is the largest value of $|\phi|$ over the complete maneuver. The tracking error is summarized using the root-mean-square error

$$\mathrm{RMSE}_\phi = \sqrt{\frac{1}{N}\sum_{i=1}^{N}(\phi_i - G_\phi a_{y,i})^2}, \tag{5.1}$$

where G_ϕ is the target roll gradient. For the passive baseline, the RMSE is computed relative to the +4 deg/g reference line, since this reference is used as the comparison target in Fig. 5.2.

Table 5.1 summarizes the roll-gradient responses obtained from the CarMaker simulations. The passive vehicle with anti-roll bar gives a fitted roll gradient of 4.32 deg/g for the baseline parameter set, which is slightly higher than the 4 deg/g reference used for comparison. At 0.7 g lateral acceleration, the passive vehicle reaches a roll angle of 3.06 deg, while the active +4 deg/g case reaches 2.74 deg.

In contrast, the active suspension controller keeps the fitted roll gradients close to the commanded values. The active +4 deg/g case gives a fitted gradient of 3.98 deg/g, the active 0 deg/g case gives almost zero roll response, and the active −4 deg/g case achieves a fitted gradient of −4.06 deg/g. The key advantage of the active controller in this comparison is therefore its ability to track different roll-gradient targets without retuning the passive mechanical parameters.

Table 5.1: Quantitative comparison of CarMaker roll-gradient responses.

Metric	Passive + ARB	Active +4	Active 0	Active −4
Fitted gradient (deg/g)	4.32	3.98	0.01	-4.06
Roll at 0.7 g (deg)	3.06	2.74	-0.01	-2.84
Max. abs. roll (deg)	3.11	2.87	0.05	2.99
RMSE to target (deg)	0.12	0.03	0.01	0.09

5.1.2 Positive Roll Gradient Control

This case evaluates the proposed active suspension system under a positive roll-gradient target of 4 deg/g, which corresponds to conventional vehicle behavior in which body roll increases with lateral acceleration.

Figure 5.3 shows the relationship between roll angle and lateral acceleration. The measured roll response stays close to the reference line across the full lateral-acceleration range, so the desired roll gradient is tracked well in steady-state cornering. The small deviations at low lateral acceleration and near the peak values are mainly associated with transient phases of the maneuver.

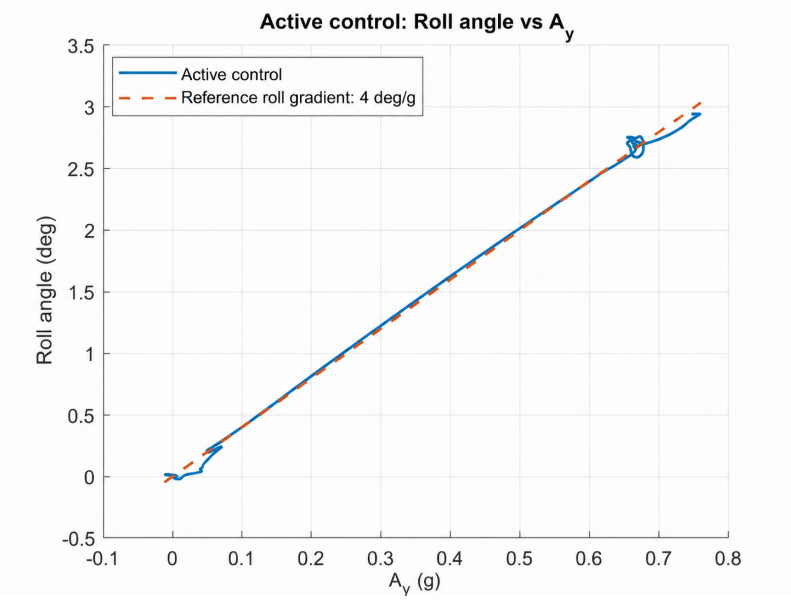

Figure 5.3: Roll angle as a function of lateral acceleration under roll motion control.

Figure 5.4 shows the suspension forces generated by the active suspension system. As lateral acceleration increases, the outer-wheel forces rise while the inner-wheel forces fall. This is the expected pattern for cornering load transfer. More specifically, the front-right (FR) and rear-right (RR) wheels carry increasing positive force, while the front-left (FL) and rear-left (RL) wheels move in the opposite direction. The force split matches the shift in vertical load from the inner side of the vehicle to the outer side.

The force profiles are smooth and follow a consistent trend, which suggests that the low-level controller tracks the high-level force demand well. The small

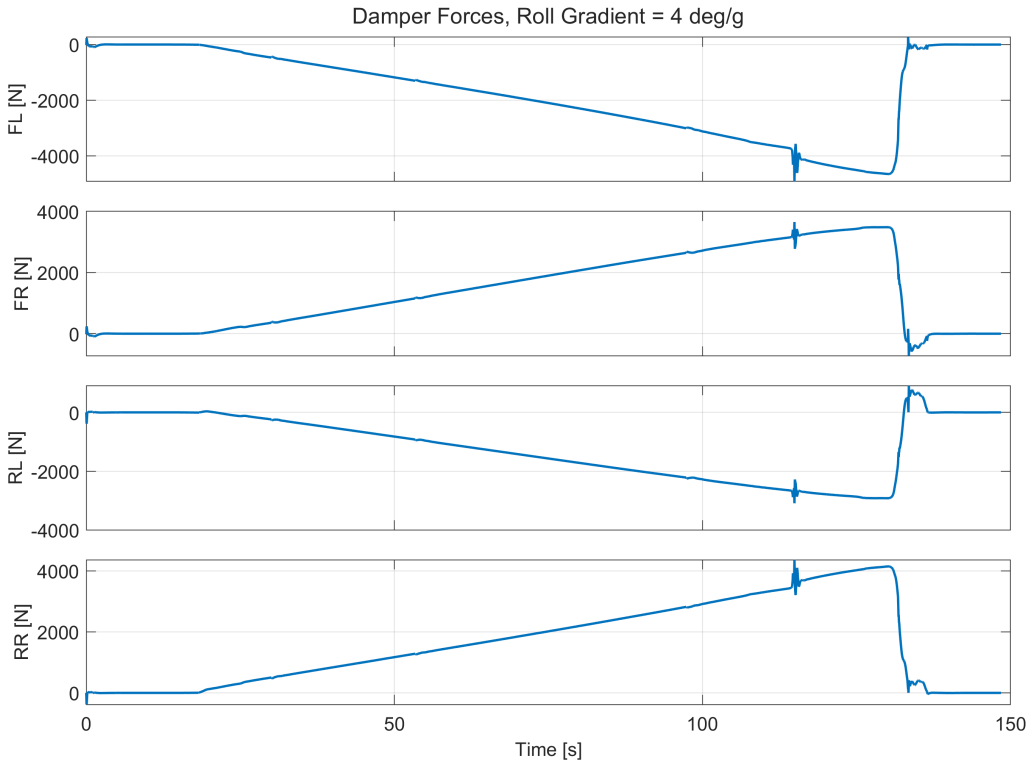

Figure 5.4: Suspension forces at the four corners (FL, FR, RL, RR) during roll motion control.

oscillations during the transitions are consistent with actuator dynamics and the changing vehicle response.

Taken together, these results show that the controller can produce the desired roll behavior without introducing unrealistic force patterns across the vehicle.

To examine actuator-level behavior more closely, Fig. 5.5 uses the front-left (FL) suspension actuator as a representative example of the force-tracking performance between the high-level controller and the low-level actuator. The upper subplot compares the desired damper force from the high-level controller with the force produced by the low-level actuator. The two traces stay close to each other through most of the maneuver, and the middle subplot shows that the tracking error remains near zero for most operating conditions.

The main mismatch appears near the force-reversal region, where the desired damper force returns rapidly toward zero. At that point the damper velocity is still relatively high, so the actuator continues to generate substantial damping force for a short time. The error is brief, and the actual force settles back to the requested value quickly after the transition.

The lower subplot shows the motor-pump activation state of the FL actuator. The pump turns on mainly when force demand and suspension activity are high. The rapid switching near the transition region is a modeling artifact: the present motor-pump model does not include practical features such as hysteresis, minimum activation time, or switching delay. Even so, the figure still gives a useful picture of the force-tracking behavior achieved by the hierarchical control framework.

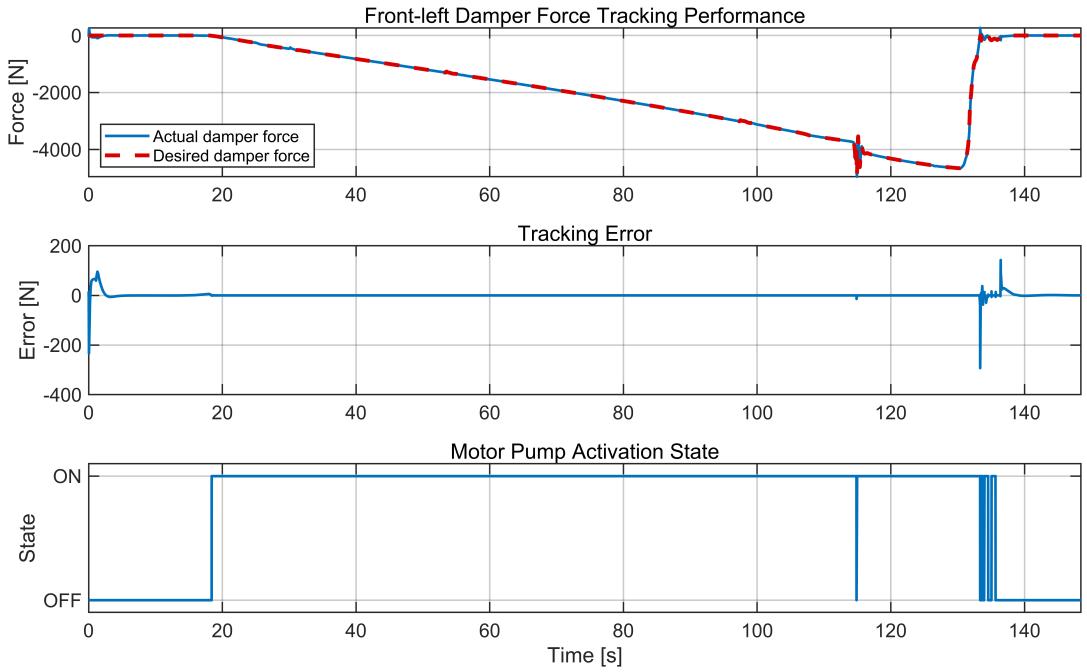

Figure 5.5: Tracking performance and motor pump activation behavior of the front-left active suspension actuator.

5.1.3 Zero Roll Gradient Control

This case examines roll suppression with a target roll gradient of 0 deg/g. The aim is to keep the body as level as possible as lateral acceleration builds during cornering.

Figure 5.6 shows roll angle as a function of lateral acceleration. The roll angle remains close to the zero reference over the tested range, with deviations below approximately 0.1 deg. This indicates that the controller suppresses the natural roll response effectively, while the remaining small deviations occur mainly at low lateral acceleration and during transient parts of the maneuver.

The corresponding suspension forces are shown in Fig. 5.7. The left and right sides develop opposing forces, generating the roll moment needed to hold the body near level instead of letting it follow the natural roll tendency.

This result sits naturally between the positive-roll and anti-roll cases. The controller is therefore not limited to the two extremes; it can also regulate the vehicle toward near-zero roll.

Figure 5.8 shows the actuator-level response for the front-left (FL) suspension unit. The desired and actual damper-force traces stay close through most of the maneuver, and the tracking error remains small except near the force reversal at the end.

The lower subplot shows that the motor pump stays active through most of the cornering phase and switches rapidly only near the final transition. That pattern is consistent with the need to generate compensating force almost continuously in order to suppress body roll.

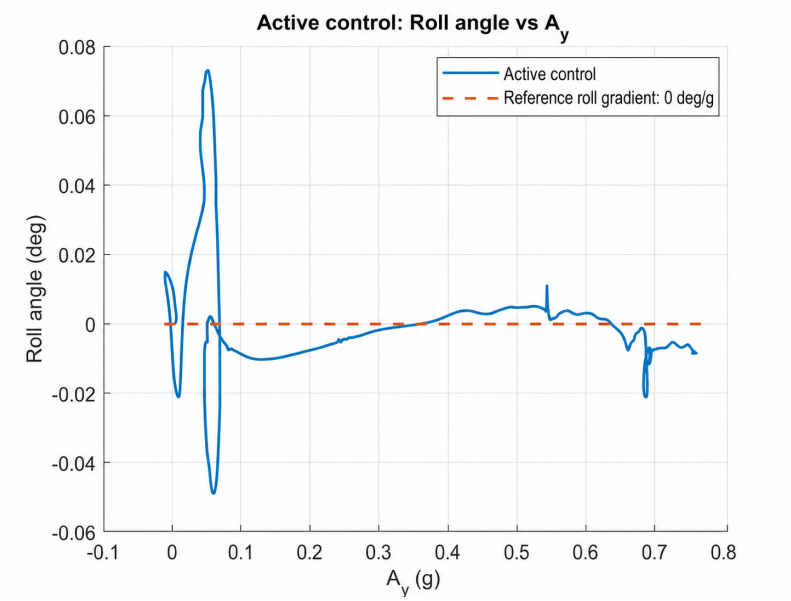

Figure 5.6: Roll angle as a function of lateral acceleration under zero roll-gradient control.

5.1.4 Negative Roll Gradient Control

This case evaluates the anti-roll strategy with a target roll gradient of -4 deg/g, meaning that the vehicle body rolls against the lateral acceleration. Figure 5.9 shows that the roll angle follows the negative reference line closely. As lateral acceleration increases, the roll angle moves in the opposite direction, so the body tilts toward the inside of the corner rather than the outside.

Figure 5.10 shows the corresponding suspension forces. The force signs remain consistent with the positive- and zero-gradient cases, but the magnitudes are larger. For example, the front-right force increases from roughly 4500 N in the zero-gradient case to above 6000 N in the negative-gradient case. The negative roll-gradient target should therefore be interpreted as a higher control-effort case rather than as a direct reversal of the vertical load transfer.

This force pattern shows that the active suspension system can generate the roll moment required to oppose the natural roll tendency. Compared with the positive-roll case, it demands more control effort.

The anti-roll case makes the controller's authority especially clear. It does not just reduce roll; it can reverse the direction of the body motion altogether.

Figure 5.11 shows the front-left (FL) actuator response in this more aggressive operating condition. Even with the larger force demand associated with the negative roll-gradient target, the low-level actuator follows the requested damper-force trajectory closely through most of the maneuver. The tracking error remains small for most of the maneuver. The largest deviations again appear near the rapid force reversal, where large suspension motion and damper velocity briefly push the actuator away from the requested value. The force returns quickly once the transition passes.

The lower subplot shows that the motor pump remains active during the peri-

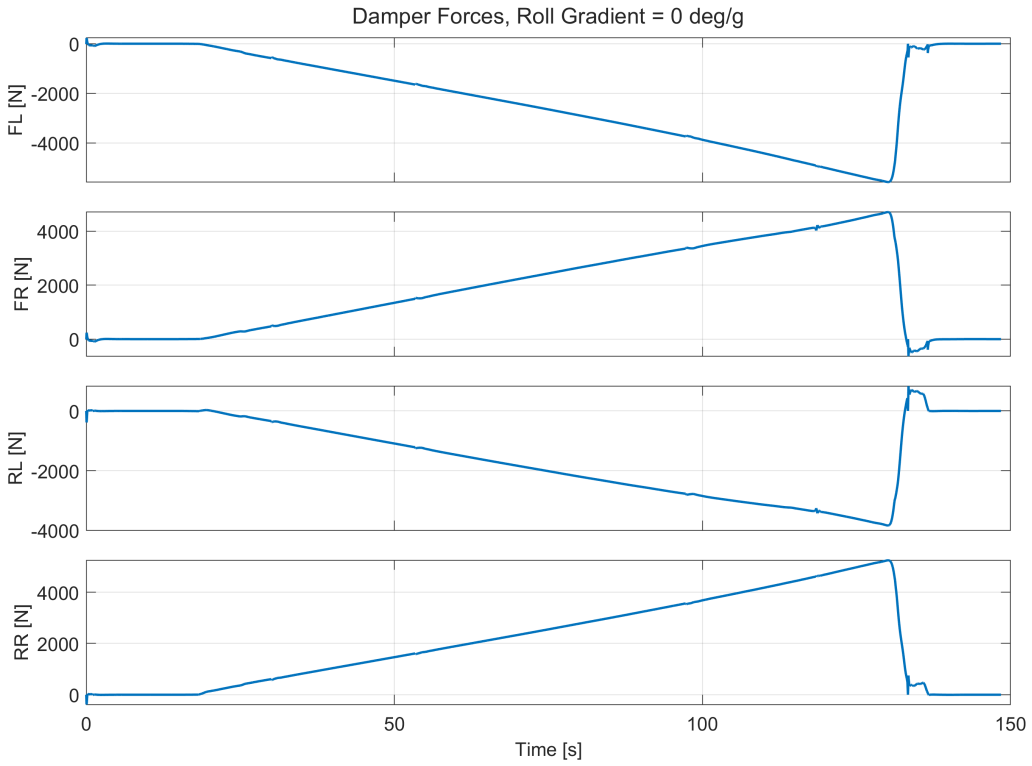

Figure 5.7: Suspension forces at the four corners (FL, FR, RL, RR) during zero roll-gradient control.

ods of highest demand in the anti-roll case. The rapid switching near the transition comes from the same idealization noted earlier: the model does not include practical switching constraints such as hysteresis or minimum activation duration. Even with that simplification, the controller remains stable and effective in this aggressive condition.

The force tracking performance of the low-level actuator model was further evaluated by comparing the desired actuator force from the high-level controller with the actual actuator force generated at each suspension corner. The force tracking error is defined as

$$e_F = F_{\text{actual}} - F_{\text{desired}}. \tag{5.2}$$

For each corner, the force tracking RMSE and maximum absolute error were calculated. In addition, the 95th percentile absolute error was used to evaluate the typical tracking error while reducing the influence of short transient peaks.

The large maximum force errors in Table 5.2 are dominated by short transient events rather than by the normal steady part of the maneuver. These peaks occur when the steering input changes rapidly and the requested actuator force reverses over a short time interval. During such high-steering-rate transitions, the damper velocity and the mode-switching logic can momentarily drive the actual force away from the requested force. This behavior is consistent with the force-reversal mismatch observed in the representative FL actuator responses in Figs. 5.5, 5.8, and 5.11. The 95th percentile errors remain close to 2 N in all three cases, which indicates that most of the maneuver has small force-tracking error, while rapid steering-

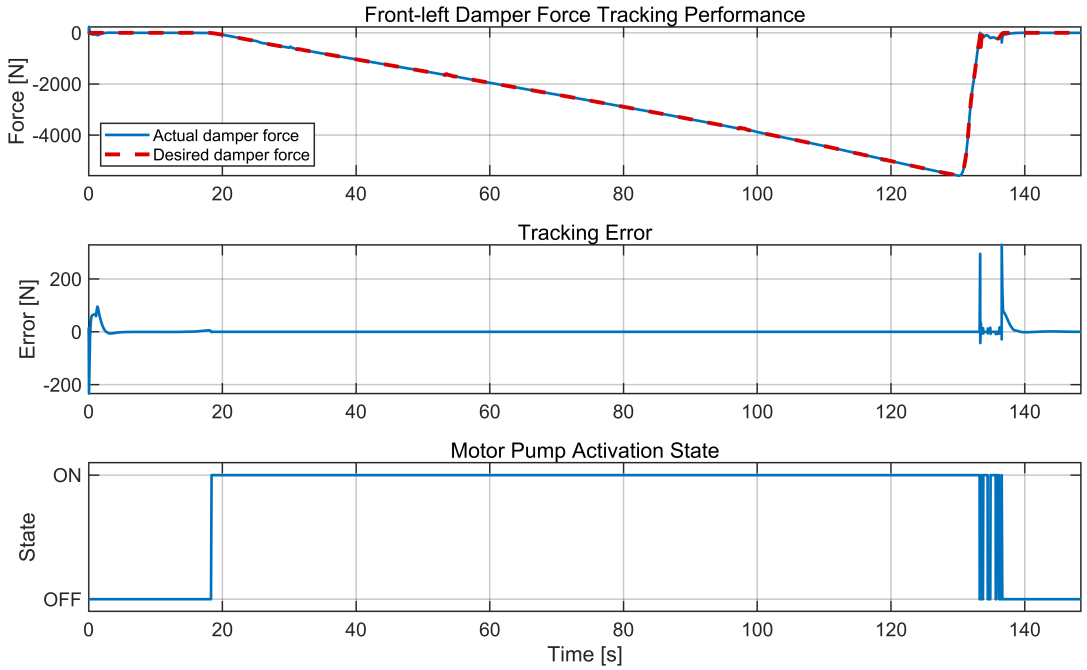

Figure 5.8: Tracking performance and motor pump activation behavior of the front-left active suspension actuator under a zero roll-gradient target of 0 deg/g.

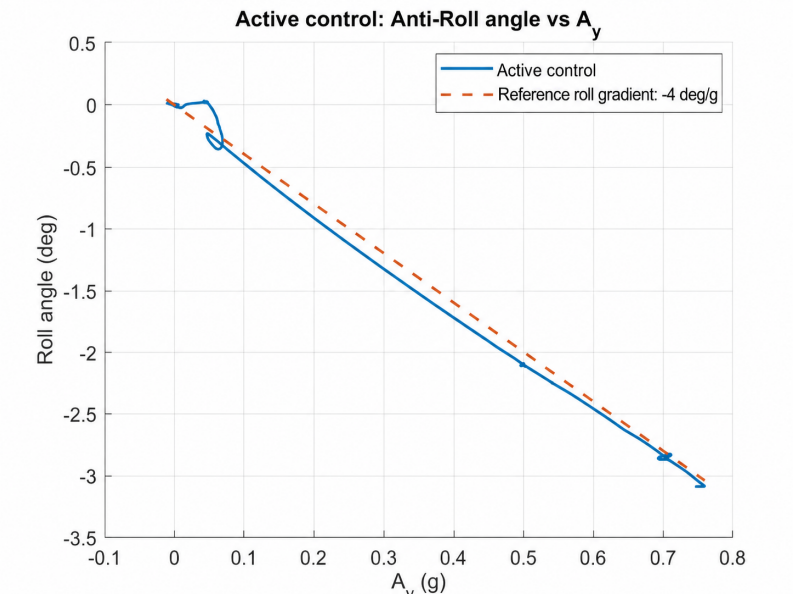

Figure 5.9: Roll angle as a function of lateral acceleration under anti-roll motion control.

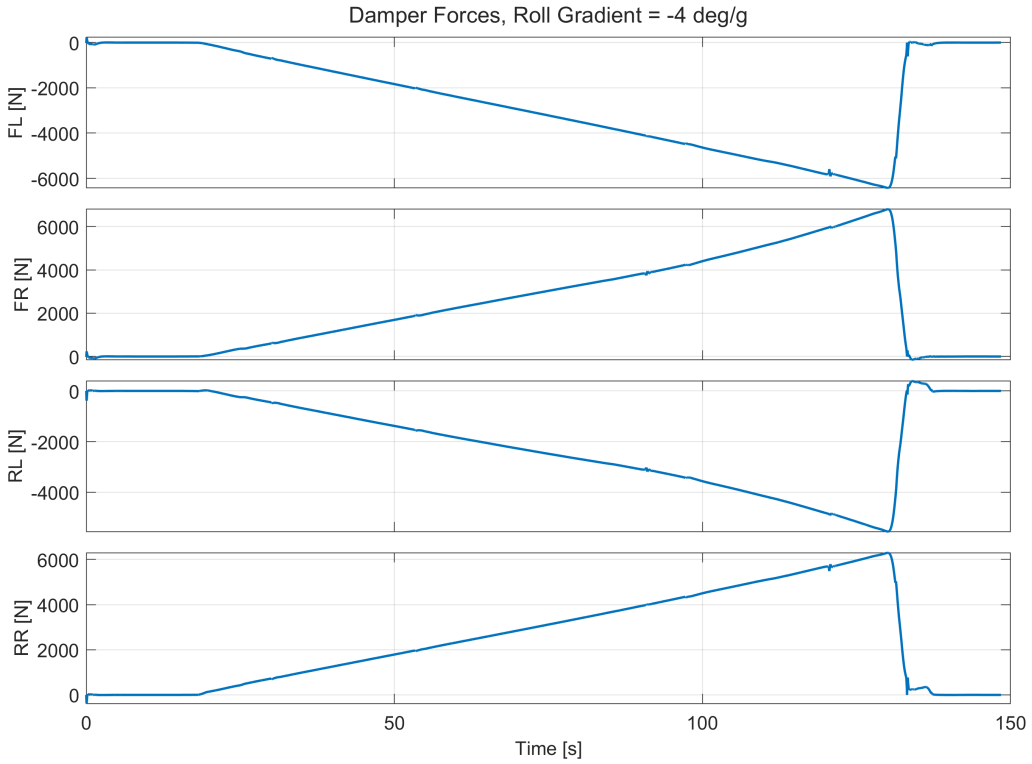

Figure 5.10: Suspension forces at the four corners (FL, FR, RL, RR) during anti-roll motion control.

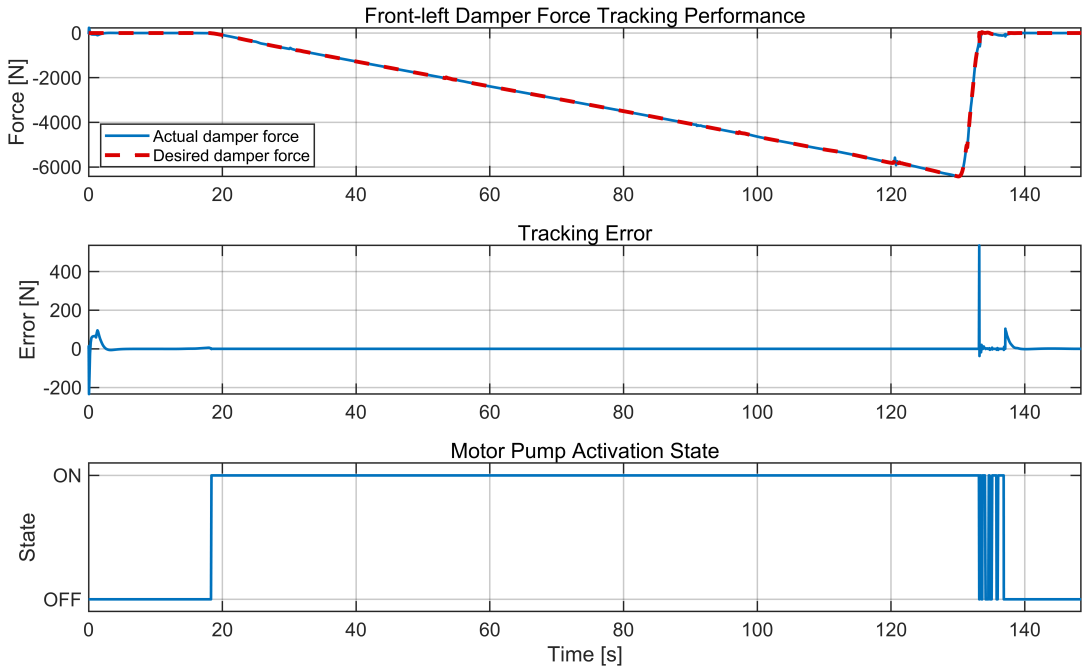

Figure 5.11: Tracking performance and motor pump activation behavior of the front-left active suspension actuator under a negative roll gradient of -4 deg/g.

induced transients remain the main limitation of the low-level actuator response.

Table 5.2: Summary of actuator force tracking errors for the active roll-gradient cases.

Metric	+4 deg/g	0 deg/g	−4 deg/g
Mean RMSE (N)	17.57	20.64	25.40
Worst-corner RMSE (N)	20.49	23.38	27.25
Max. force error (N)	4534.84	5350.68	6412.17
Mean 95th percentile error (N)	1.61	1.62	1.63
Worst 95th percentile error (N)	2.05	2.03	2.02

5.1.5 Generalized Control Demands

After evaluating the roll-gradient responses, the generalized control demands were analysed to investigate how the high-level controller behaves for the different roll-gradient targets. Figure 5.12 shows the desired roll moment $M_{\phi,\mathrm{des}}$, pitch moment $M_{\rho,\mathrm{des}}$, and vertical force $F_{z,\mathrm{des}}$ for the −4 deg/g, 0 deg/g, and +4 deg/g cases.

The roll-moment demand $M_{\phi,\mathrm{des}}$ shows the clearest difference between the three cases. The largest peak absolute roll-moment demand occurs for the −4 deg/g case, with a value of 15000 Nm. The 0 deg/g case gives an intermediate value of 11459 Nm, while the +4 deg/g case gives the lowest value of 9465.7 Nm. This is expected, since the negative roll-gradient target requires the vehicle body to roll against the natural roll direction during cornering, which demands a larger active suspension contribution.

The pitch-moment demand $M_{\rho,\mathrm{des}}$ does not follow the same trend as the roll-moment demand. The largest pitch-moment demand occurs in the 0 deg/g case, while the −4 deg/g case gives the lowest value. This indicates that the pitch response is affected by the transient vehicle motion during the manoeuvre, although pitch control is not the main objective of this study. The vertical force demand $F_{z,\mathrm{des}}$ remains almost unchanged for the three cases, with peak values around 394–397 N. This shows that the heave-related demand is only weakly influenced by the selected roll-gradient target.

Table 5.3 summarizes the peak absolute values of the generalized control demands. The quantitative comparison confirms that the selected roll-gradient target mainly affects the required roll moment, while the vertical force demand remains nearly constant.

Table 5.3: Peak absolute generalized control demands for the CarMaker roll-gradient cases.

Roll-gradient target	$\lvert M_{\phi,\mathrm{des}}\rvert_{\max}$ [Nm]	$\lvert M_{\rho,\mathrm{des}}\rvert_{\max}$ [Nm]	$\lvert F_{z,\mathrm{des}}\rvert_{\max}$ [N]
−4 deg/g	15000	1796.2	397.44
0 deg/g	11459	2994.8	394.48
+4 deg/g	9465.7	2904.2	394.37

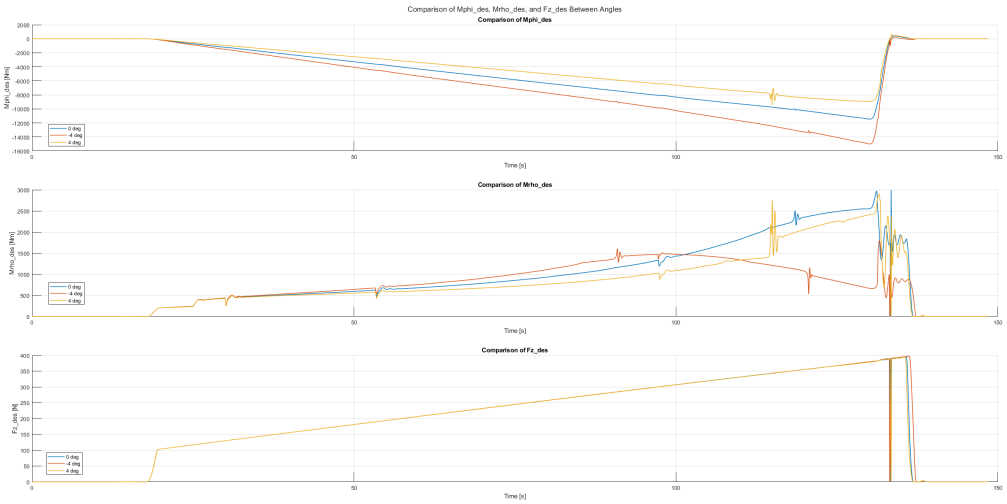

Figure 5.12: Generalized control demands $M_{\phi,\mathrm{des}}$, $M_{\rho,\mathrm{des}}$, and $F_{z,\mathrm{des}}$ for the CarMaker roll-gradient cases.

The peak-time results show that the largest roll-moment demands for the -4 deg/g and 0 deg/g cases occur around $t = 130$ s. For the $+4$ deg/g case, the peak roll-moment demand occurs earlier, around $t = 115$ s. These peaks correspond to transient parts of the manoeuvre where the control demand changes rapidly.

5.1.6 Required MPU Flow

The required motor-pump-unit (MPU) flow was also analysed to evaluate the low-level actuator effort needed to realize the requested suspension forces. Figure 5.13 shows the required MPU flow at the four suspension corners for the three roll-gradient targets.

The results show that the required MPU flow depends strongly on the selected roll-gradient target. The -4 deg/g case produces the largest actuator demand, especially near the transient part of the manoeuvre. The $+4$ deg/g case generally requires the lowest flow demand, while the 0 deg/g case remains between the two cases. This trend is consistent with the generalized roll-moment demand, where the negative roll-gradient case requires the largest control effort.

The sign of the required MPU flow also shows the expected left–right actuator coordination. The left-side actuators mainly require positive flow, whereas the right-side actuators mainly require negative flow. This indicates that the actuators on the two sides of the vehicle work in opposite directions to generate the required roll moment.

Table 5.4 summarizes the peak absolute required MPU flow for each suspension corner. The values are presented in L/min. The quantitative comparison confirms that the -4 deg/g case is the most demanding case from an actuator perspective. The largest peak occurs at the front-right actuator, with a value of 198.1 L/min, followed by the rear-right actuator with 172.2 L/min. The 0 deg/g case requires lower peak flow than the -4 deg/g case, while the $+4$ deg/g case has the lowest

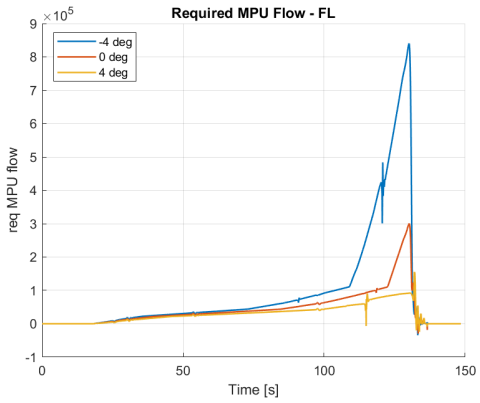

(a) Front-left

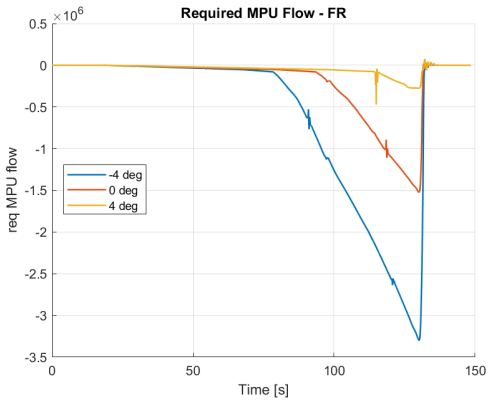

(b) Front-right

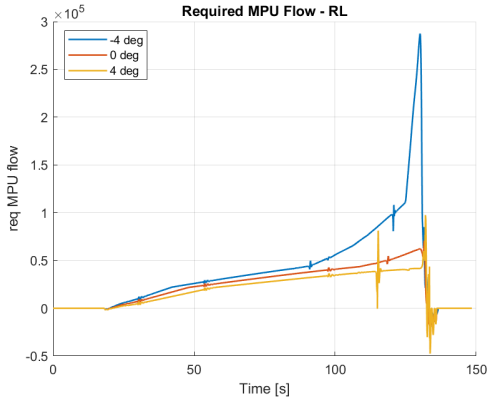

(c) Rear-left

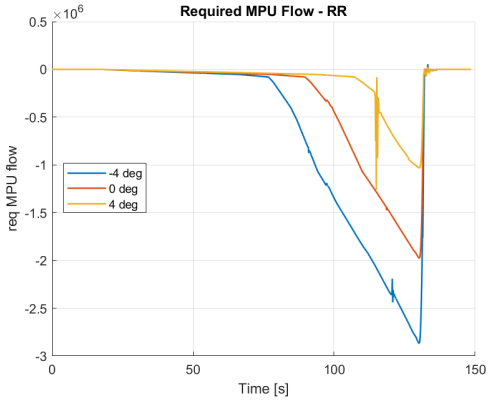

(d) Rear-right

Figure 5.13: Required MPU flow at the four suspension corners for the CarMaker roll-gradient cases.

overall demand.

Table 5.4: Peak absolute required MPU flow, $\left|Q_{\text{pump}}^{\text{req}}\right|_{\text{max}}$, for the CarMaker roll-gradient cases.

Roll-gradient target	FL [L/min]	FR [L/min]	RL [L/min]	RR [L/min]
−4 deg/g	50.4	198.1	17.2	172.2
0 deg/g	18.0	91.5	4.2	118.7
+4 deg/g	9.3	28.3	5.9	75.7

The peak-time results show that the largest flow demands for the −4 deg/g and 0 deg/g cases occur around $t = 130$ s. This corresponds to the transient part of the manoeuvre, where the controller demand changes rapidly as the vehicle returns toward straight-line driving. Overall, these results show that roll-gradient shaping affects not only the vehicle roll response, but also the low-level actuator effort required to realize the desired body motion. Therefore, aggressive roll-gradient targets should be evaluated together with the required actuator flow and implementation feasibility.

5.2 VI-CRT Simulator Results

The VI-CRT simulator is used to evaluate the controller under real-time, driver-in-the-loop operation. The tests are not completely free driving; the driver follows a prescribed set of cornering maneuvers that includes left cornering, right cornering, and a left-to-right steering transition. Unlike the predefined CarMaker maneuver, the VI-CRT tests include human steering input and therefore contain steering reversals, path variation, and transient operating points. The results are therefore interpreted mainly from the relationship between lateral acceleration and roll angle, rather than from exact time repeatability. For each case, the left- and right-cornering branches are shown separately and together. The grey points show the raw simulator data, the black curve shows the filtered mean response, the red dashed line gives the fitted roll gradient, and the blue dotted line shows the reference gradient.

5.2.1 Passive Reference

The passive VI-CRT result is first used as a reference for the uncontrolled roll behavior. As shown in Fig. 5.14, the passive vehicle has a nearly linear roll-angle response over the tested lateral-acceleration range. The fitted gradient is approximately 4.63 deg/g when the two cornering directions are considered together. The left- and right-cornering branches give similar fitted gradients of 4.62 deg/g and 4.64 deg/g, respectively, which indicates that the passive response is approximately symmetric in the VI-CRT test.

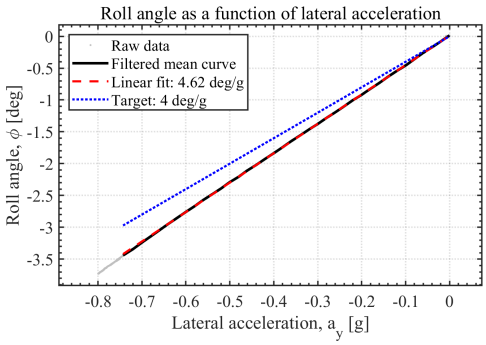

(a) Left-cornering branch.

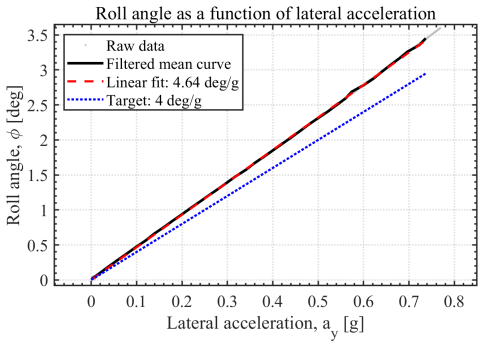

(b) Right-cornering branch.

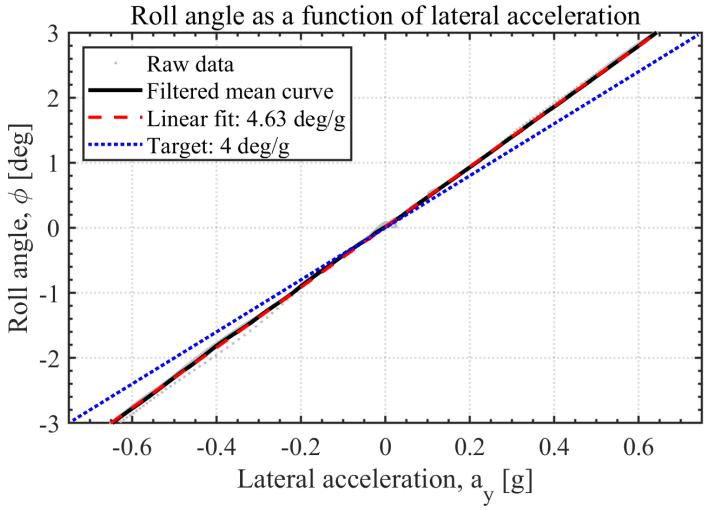

(c) Combined left- and right-cornering response.

Figure 5.14: VI-CRT passive reference roll-angle response.

This passive case provides the baseline for the active-control cases. The fitted passive gradient is slightly higher than the 4 deg/g reference line used in the comparison, meaning that the passive body roll increases somewhat faster than the selected positive-gradient target. More importantly, the passive response can only produce conventional roll behavior; it cannot reduce the gradient toward zero or reverse the roll direction.

5.2.2 Positive Roll Gradient Control

Figure 5.15 shows the VI-CRT result for the positive roll-gradient target of +4 deg/g. The combined response gives a fitted gradient of approximately 3.78 deg/g, while the separated branches give 3.72 deg/g and 3.90 deg/g. The controller therefore produces a roll response close to the commanded positive gradient in both cornering directions.

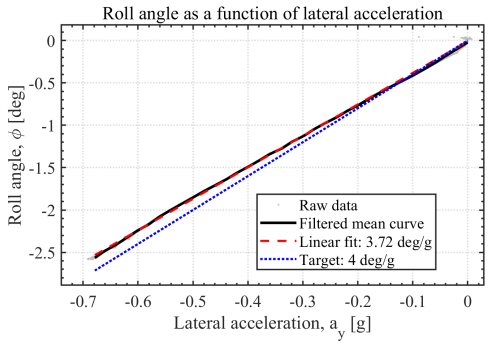

(a) Left-cornering branch.

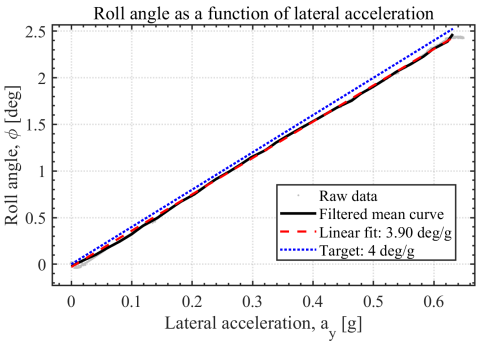

(b) Right-cornering branch.

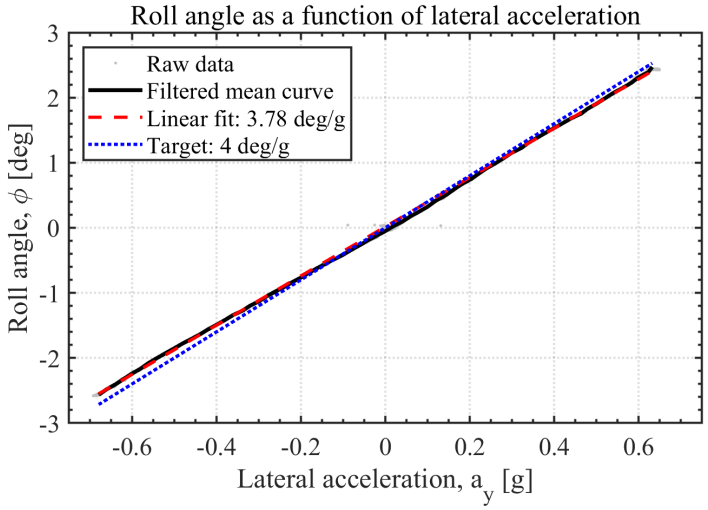

(c) Combined left- and right-cornering response.

Figure 5.15: VI-CRT simulator roll-angle response for the positive roll-gradient target of +4 deg/g.

Compared with the passive reference, the +4 deg/g controller reduces the fitted gradient from 4.63 deg/g to 3.78 deg/g. The reduction is modest, because the target is close to the passive VI-CRT behavior, but the result still shows that the controller can shape the roll response toward the selected positive target while maintaining a consistent relationship between lateral acceleration and roll angle.

5.2.3 Zero Roll Gradient Control

The zero-gradient case tests whether the active suspension can suppress body roll during cornering. The result is shown in Fig. 5.16. The combined fitted gradient is approximately 0.27 deg/g. The separated branches give 0.08 deg/g and 0.19 deg/g, showing that the filtered roll response remains close to the zero-gradient target in both cornering directions.

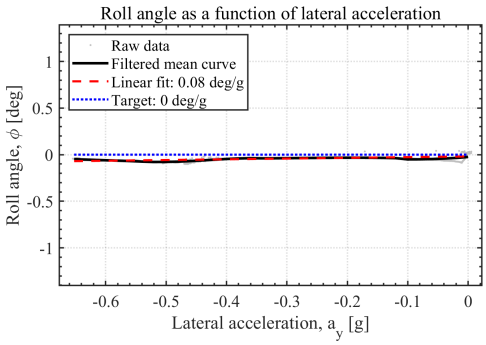

(a) Left-cornering branch.

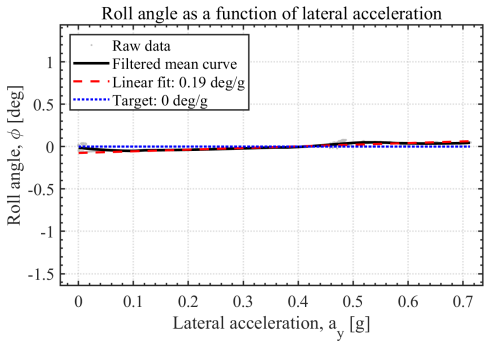

(b) Right-cornering branch.

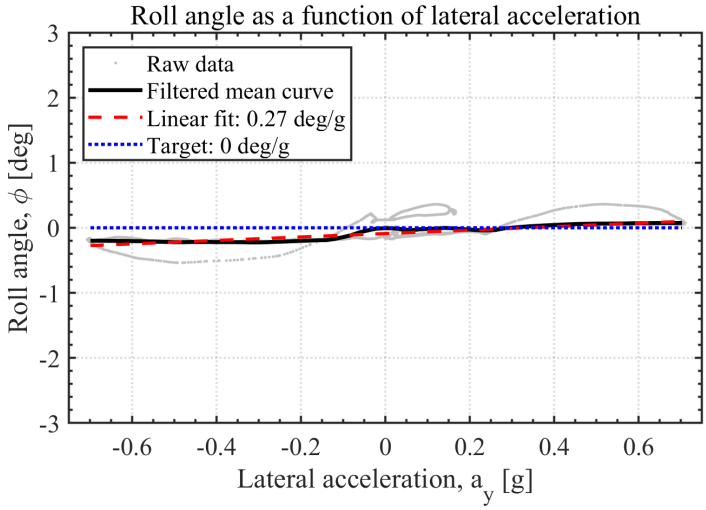

(c) Combined left- and right-cornering response.

Figure 5.16: VI-CRT simulator roll-angle response for the zero roll-gradient target of 0 deg/g.

Relative to the passive reference, the zero-gradient controller strongly reduces the roll-angle sensitivity to lateral acceleration. The raw data still contain some spread, especially around steering reversals and transient parts of the manually driven maneuver, but the filtered response remains close to zero roll angle across most of the tested range. This confirms that the controller can keep the vehicle body close to level under driver-in-the-loop operation.

5.2.4 Negative Roll Gradient Control

The negative-gradient case tests whether the controller can produce anti-roll behavior, where the vehicle body tilts opposite to the passive roll direction. Figure 5.17 shows the VI-CRT result for the target of -4 deg/g. The combined fitted gradient is approximately -2.79 deg/g, while the separated branches give -3.02 deg/g and -3.17 deg/g. The fitted gradients are smaller in magnitude than the commanded value, but their sign is clearly negative.

The result demonstrates a clear reversal compared with the passive and positive-gradient cases. Positive lateral acceleration is associated with negative roll angle,

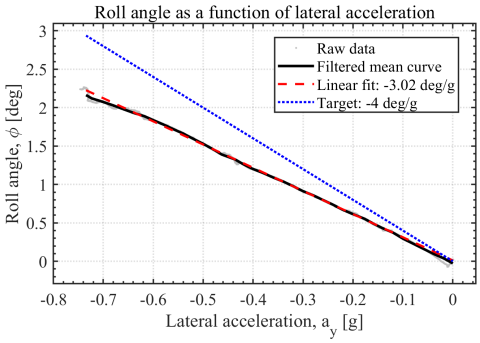

(a) Left-cornering branch.

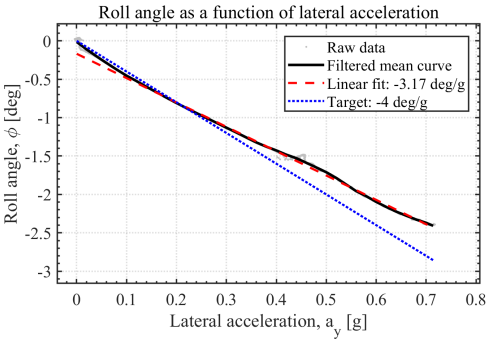

(b) Right-cornering branch.

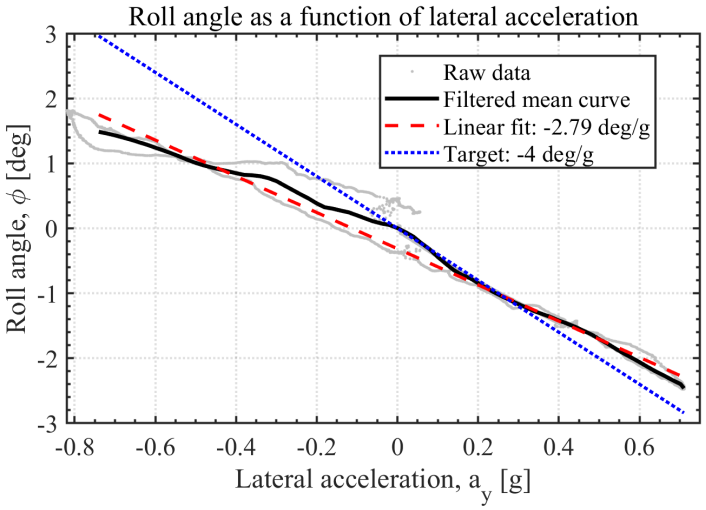

(c) Combined left- and right-cornering response.

Figure 5.17: VI-CRT simulator roll-angle response for the negative roll-gradient target of -4 deg/g.

while negative lateral acceleration is associated with positive roll angle. The controller does not fully reach the -4 deg/g target, especially when the two cornering directions are combined, but it still changes the dominant roll behavior from conventional roll to anti-roll. The remaining error is consistent with the more demanding actuator-force requirements and transient driver inputs in the real-time simulator.

Taken together, the VI-CRT results show that the controller preserves the intended ordering of the roll-gradient targets under driver-in-the-loop operation. The passive reference gives a conventional positive roll gradient of about 4.63 deg/g. The active controller then produces a near-target positive gradient of 3.78 deg/g, suppresses the roll response to about 0.27 deg/g in the zero-gradient case, and reverses the roll direction to about -2.79 deg/g in the negative-gradient case. This confirms that the active suspension can shape the roll behavior in the real-time simulator, while also showing that the negative-gradient target is the most difficult case to track exactly.

6

Conclusions and Future Work

6.1 Conclusions

This thesis examined roll-motion control for a fully active suspension system using a hierarchical control architecture. The work combined a high-level body-motion controller, a force-allocation step, and a low-level actuator controller based on lookup tables and mode-switching logic. The main conclusion is that this structure can shape vehicle roll behavior by tracking prescribed roll-gradient targets, provided that the vehicle-level motion objective and the actuator-level force realization are considered together.

RQ1 asked how a high-level controller can be designed to generate suspension-force requests for shaping roll behavior. This was addressed by combining lateral-acceleration-based feedforward control with PI feedback control for roll, pitch, and heave motion. The resulting generalized force and moment demands were converted into corner suspension-force requests through the input-decoupling and force-allocation formulation. This structure allowed the desired roll behavior to be specified directly through positive, zero, and negative roll-gradient targets.

RQ2 asked how a low-level actuator controller can convert the requested suspension forces into feasible actuator commands. This was addressed using supplier-based lookup tables, mode-switching logic, and pump-flow calculation. The low-level controller selected the required damper-valve current and motor-pump operation based on requested force, damper velocity, and operating mode. The force-tracking results show that the requested forces were followed well in most operating regions, with the main deviations appearing near rapid force reversals and mode transitions.

RQ3 asked how accurately the proposed control system can track different roll-gradient targets in CarMaker and VI-CRT. In CarMaker, the active controller reproduced the positive, zero, and negative roll-gradient targets closely, with fitted gradients of 3.98 deg/g, 0.01 deg/g, and -4.06 deg/g, respectively. In VI-CRT, the same ordering of roll behavior was preserved under driver-in-the-loop operation: the $+4$ deg/g case remained close to the commanded positive gradient, the zero-gradient case kept the body close to level, and the -4 deg/g case reversed the roll direction. The negative-gradient case was the most demanding condition and did not fully reach the commanded magnitude in VI-CRT, but the dominant anti-roll behavior was still achieved.

The generalized control-demand and required MPU-flow results further show that actuator effort depends strongly on the selected roll-gradient target. The negative roll-gradient case required the largest control effort and the highest pump-flow

demand, especially during transient parts of the maneuver. This confirms that aggressive anti-roll behavior is more demanding not only at the vehicle-motion level, but also at the actuator level.

Overall, the results show that roll-gradient shaping for a fully active suspension system is not only a high-level vehicle-control problem. The achievable behavior also depends on actuator mapping, mode switching, pump-flow demand, and force-tracking performance at the low level. The proposed framework therefore provides a connected approach for evaluating roll-motion control from body-level objectives down to actuator-level implementation.

6.2 Future Work

The next steps follow naturally from the current results. At the high-level control, it would be worth testing controllers such as linear quadratic regulator (LQR) and model predictive control (MPC). Those methods may handle multi-objective trade-offs and control constraints more cleanly than the present PI-based design, especially when roll, pitch, heave, and actuator limits all matter at the same time.

At the low-level control, the motor-pump model should be made more realistic. In the current work, the pump behavior is simplified, which is why rapid switching appears in some transients. A more practical implementation should include delays, hysteresis, minimum activation times, flow limits, pressure dynamics, and other limitations that come with actual hardware. The actuator energy consumption should also be evaluated, especially because the MPU-flow results show that negative roll-gradient control requires higher actuator demand.

The obvious final step is deployment on a real vehicle. That is where the controller would face the disturbances and constraints that matter most in practice: sensor noise, road irregularities, actuator nonlinearities, thermal effects, and hardware limits. Real-vehicle testing would therefore give a much clearer picture of how robust and practical the proposed control strategy really is.

Bibliography

[1] T. D. Gillespie, *Fundamentals of Vehicle Dynamics*. Warrendale, PA: Society of Automotive Engineers, 1992 (cit. on pp. 1, 12, 13, 15).

[2] R. S. Sharp and D. A. Crolla, "Road vehicle suspension system design–a review," *Vehicle System Dynamics*, vol. 16, no. 3, pp. 167–192, 1987 (cit. on p. 1).

[3] H. E. Tseng and D. Hrovat, "State of the art survey: Active and semi-active suspension control," *Vehicle System Dynamics*, vol. 53, no. 7, pp. 1034–1062, 2015 (cit. on pp. 1, 4).

[4] W. Cho, J. Yoon, J. Kim, J. Hur, and K. Yi, "An investigation into unified chassis control scheme for optimised vehicle stability and manoeuvrability," *Vehicle System Dynamics*, vol. 46, no. sup1, pp. 87–105, 2008. DOI: 10.1080/00423110701882330 (cit. on p. 1).

[5] R. N. Jazar, *Vehicle Dynamics: Theory and Application*, 3rd. New York, NY: Springer, 2017 (cit. on pp. 1, 15).

[6] S. Solmaz, M. Corless, and R. Shorten, "A methodology for the design of robust rollover prevention controllers for automotive vehicles with active steering," *International Journal of Control*, vol. 80, no. 11, pp. 1763–1779, 2007. DOI: 10.1080/00207170701473987 (cit. on pp. 1, 4).

[7] M. R. Stone and M. A. Demetriou, "Modeling and simulation of vehicle ride and handling performance," in *Proceedings of the 15th IEEE International Symposium on Intelligent Control (ISIC 2000)*, Patras, Greece, 2000, pp. 109–114 (cit. on p. 1).

[8] A. Hosseinian Ahangarnejad, "Integrated control of active vehicle chassis control systems," Ph.D. dissertation, Politecnico di Milano, Milan, Italy, 2018 (cit. on p. 1).

[9] S. Ikenaga, F. L. Lewis, J. Campos, and L. Davis, "Active suspension control of ground vehicle based on a full-vehicle model," in *Proceedings of the 2000 American Control Conference*, vol. 6, IEEE, 2000, pp. 4019–4024 (cit. on pp. 1, 10).

[10] Z. Feng, M. Yu, S. A. Evangelou, I. M. Jaimoukha, and D. Dini, "Feedforward pid control of full-car with parallel active link suspension for improved chassis attitude stabilization," *arXiv preprint arXiv:2203.04162*, 2022 (cit. on pp. 2, 23, 28).

[11] D. Hrovat, "Survey of advanced suspension developments and related optimal control applications," *Automatica*, vol. 33, no. 10, pp. 1781–1817, 1997 (cit. on pp. 3, 4).

[12] R. Rajamani, *Vehicle Dynamics and Control*. New York: Springer, 2006 (cit. on p. 3).

[13] W. Sun, H. Gao, and O. Kaynak, "Adaptive backstepping control for active suspension systems with actuator saturation," *IEEE Transactions on Industrial Electronics*, vol. 60, no. 12, pp. 5580–5589, 2013 (cit. on p. 3).

[14] M. M. Morato, M. Q. Nguyen, O. Sename, and L. Dugard, "Design of a fast real-time lpv model predictive control system for semi-active suspension control of a full vehicle," *Journal of the Franklin Institute*, vol. 356, no. 3, pp. 1196–1224, 2019. DOI: 10.1016/j.jfranklin.2018.11.016 (cit. on p. 4).

[15] S. Yim, K. Jeon, and K. Yi, "Design of a robust controller for rollover prevention with active suspension and differential braking," *Journal of Mechanical Science and Technology*, vol. 26, no. 1, pp. 213–222, 2012 (cit. on p. 4).

[16] J. Theunissen, A. Tota, P. Gruber, M. Dhaens, and A. Sorniotti, "Preview-based techniques for vehicle suspension control: A state-of-the-art review," *Annual Reviews in Control*, vol. 51, pp. 206–235, 2021 (cit. on pp. 4, 23).

[17] D. Wang, D. Zhao, M. Gong, and B. Yang, "Research on robust model predictive control for electro-hydraulic servo active suspension systems," *IEEE Access*, vol. 6, pp. 3231–3240, 2018. DOI: 10.1109/ACCESS.2017.2787663 (cit. on p. 4).

[18] J. Sun and K. Zhao, "Adaptive neural network sliding mode control for active suspension systems with electrohydraulic actuator dynamics," *International Journal of Advanced Robotic Systems*, vol. 17, no. 4, 2020. DOI: 10.1177/1729881420941986 (cit. on p. 4).

[19] J. Lee, K. Oh, and K. Yi, "A novel approach to design and control of an active suspension using linear pump control-based hydraulic system," *Proceedings of the Institution of Mechanical Engineers, Part D: Journal of Automobile Engineering*, vol. 234, no. 5, pp. 1224–1248, 2020. DOI: 10.1177/0954407019882223 (cit. on p. 4).

[20] C. Poussot-Vassal, C. Spelta, O. Sename, S. M. Savaresi, and L. Dugard, "Survey and performance evaluation on some automotive semi-active suspension control methods: A comparative study on a single-corner model," *Annual Reviews in Control*, vol. 36, no. 1, pp. 148–160, 2012 (cit. on p. 4).

[21] United Nations, *Transforming our world: The 2030 agenda for sustainable development*, https://sdgs.un.org/2030agenda, Accessed: 2026-05-13, 2015 (cit. on pp. 4, 5).

[22] H. Heisler, *Advanced Vehicle Technology*, 2nd. Oxford: Butterworth-Heinemann, 2002, ISBN: 978-0-7506-5131-8 (cit. on pp. 13, 15).

[23] D. Cao, X. Song, and M. Ahmadian, "Editors' perspectives: Road vehicle suspension design, dynamics, and control," *Vehicle System Dynamics*, vol. 49, no. 1-2, pp. 3–28, 2011 (cit. on p. 16).

[24] ZF Friedrichshafen AG, *sMOTION – Active Suspension System*, https://www.zf.com/products/en/cars/products_64239.html, Accessed: 2026-05-19 (cit. on p. 18).

[25] P. Gáspár and Z. Szabó, "Design of a hierarchical controller for suspension systems," in *Robust Control and Linear Parameter Varying Approaches*, ser. Lecture Notes in Control and Information Sciences, O. Sename, P. Gaspar, and J. Bokor, Eds., vol. 437, Berlin, Heidelberg: Springer, 2013, pp. 311–328. DOI: 10.1007/978-3-642-36110-4_12 (cit. on p. 21).

[26] B. Lennartson, *Reglerteknikens grunder*, Swedish, 4th ed. Lund, Sweden: Studentlitteratur, 2000, ISBN: 9789144024165 (cit. on pp. 23, 24).

[27] D. Liberzon and A. S. Morse, "Basic problems in stability and design of switched systems," *IEEE Control Systems Magazine*, vol. 19, no. 5, pp. 59–70, 1999. DOI: 10.1109/37.793443 (cit. on p. 25).

[28] E. O. Ericksen, C. P. Cox, P. Tsiaras, M. Larson, M. Galasso, and M. McLellan, "Method and apparatus for an adjustable damper," US10821795B2, Assigned to Fox Factory, Inc., Nov. 2020 (cit. on p. 34).

[29] VI-grade GmbH, *VI-CarRealTime*, https://www.vi-grade.com/en/products/vi-carrealtime/, Accessed: 2026-05-29 (cit. on pp. 41, 42).

[30] The MathWorks, Inc., *VI-DriveSim, VI-CarRealTime, VI-BikeRealTime, VI-Automotive, VI-Motorcycle, VI-Aircraft, VI-Rail*, https://www.mathworks.com/products/connections/product_detail/vi-automotive-vi-aircraft-vi-rail.html, Accessed: 2026-05-29 (cit. on pp. 41, 42).

A

Appendix 1

This appendix presents supplementary time-history signals obtained from the VI-CRT simulator tests. The purpose of these plots is to support the roll-gradient results discussed in the main results chapter by showing the corresponding vehicle input, body-motion, suspension-displacement, damper-velocity, damper-force, and wheel-displacement responses. Although these signals are not used as the primary performance indicators, they provide additional evidence that the observed roll-gradient behavior is supported by physically consistent suspension and actuator responses.

The comparison plots include the passive reference case and the three active roll-gradient targets: +4 deg/g, 0 deg/g, and -4 deg/g. For the detailed corner-level suspension signals, the -4 deg/g case is selected as the representative case because it produces the most demanding control condition and requires the largest actuator contribution from the active suspension system.

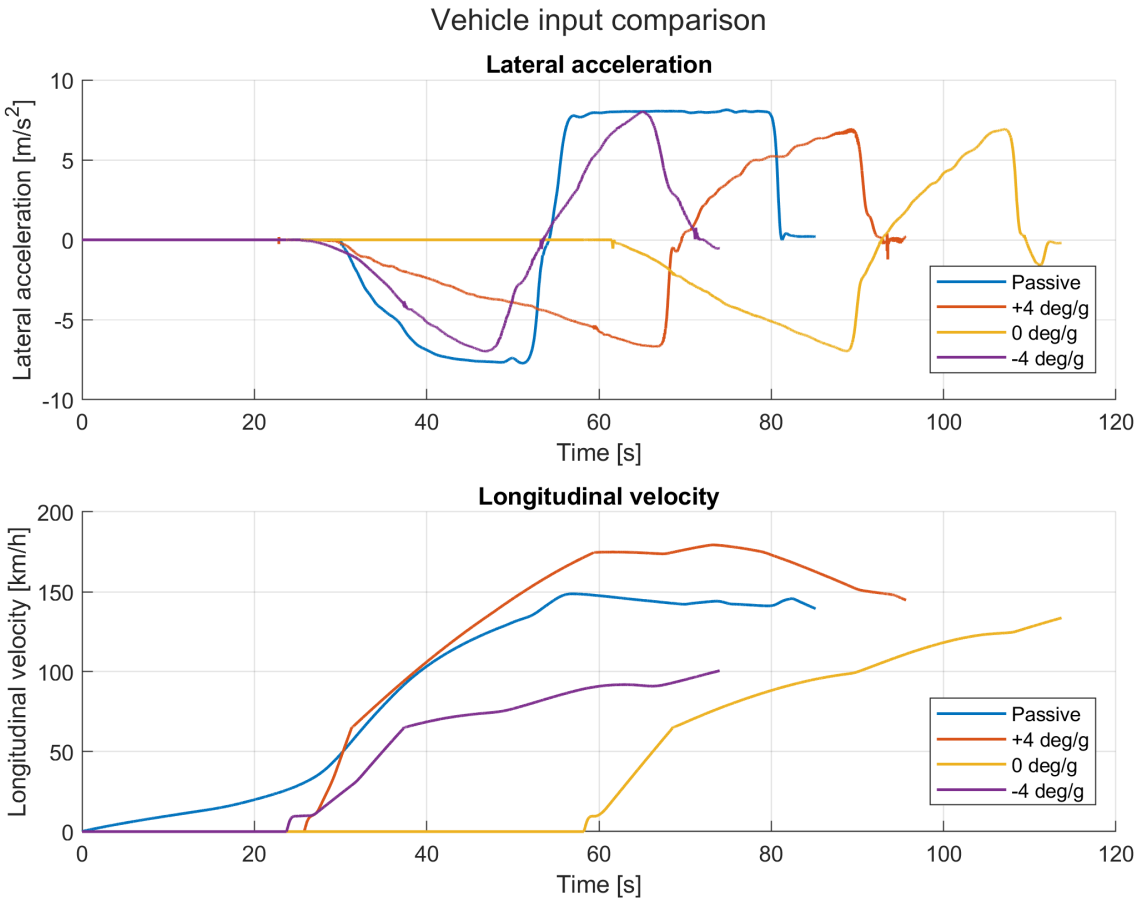

Figure A.1: Vehicle input comparison from the VI-CRT simulations for the passive reference and active roll-gradient cases. The upper subplot shows lateral acceleration, while the lower subplot shows longitudinal velocity. These signals define the driving conditions under which the roll-gradient responses were evaluated.

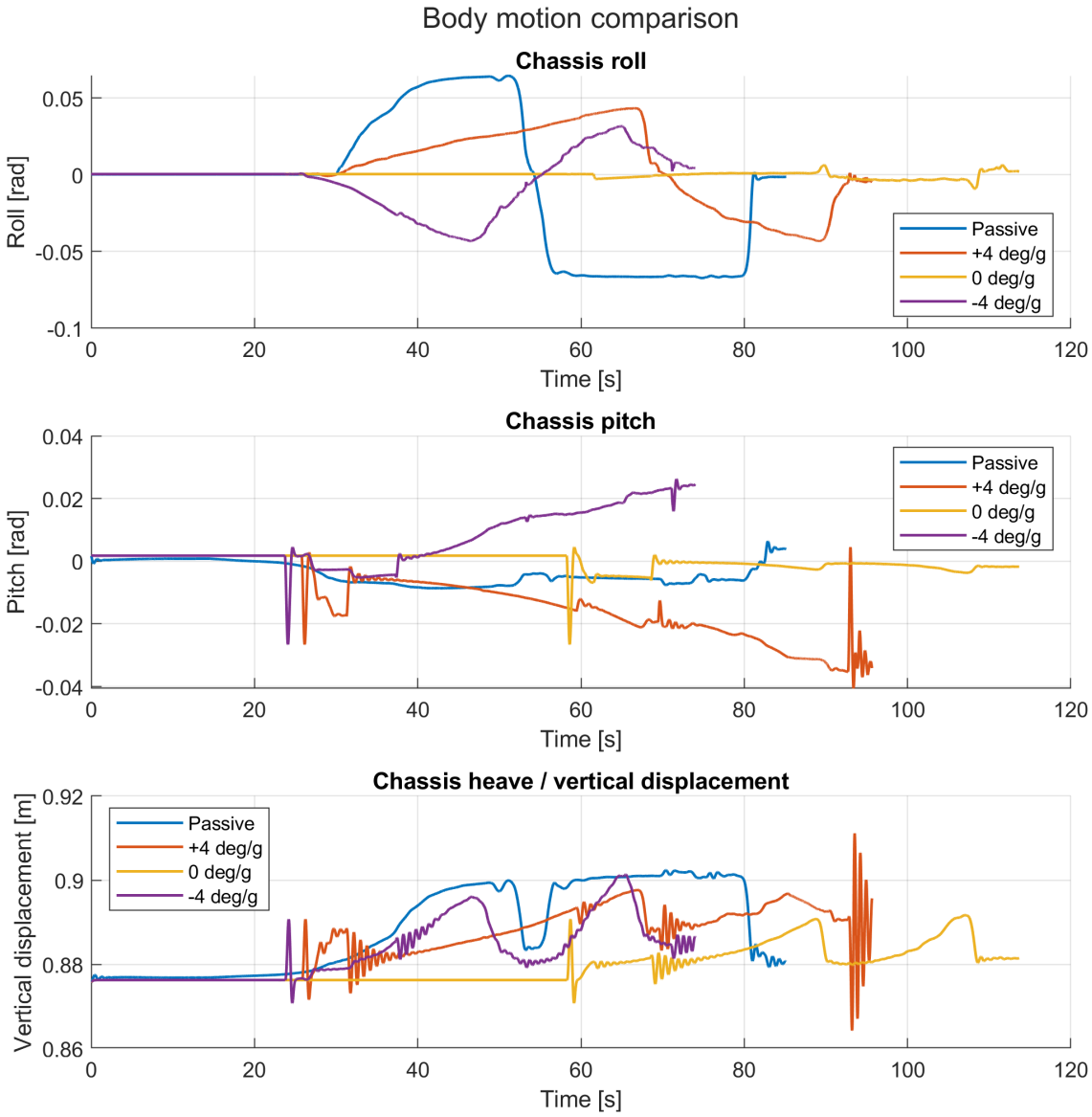

Figure A.2: Body-motion comparison from the VI-CRT simulations for the passive reference and active roll-gradient cases. The figure shows chassis roll, pitch, and heave responses. The roll response varies according to the selected roll-gradient target, while the pitch and heave responses provide additional information about the overall body-motion behavior during the maneuver.

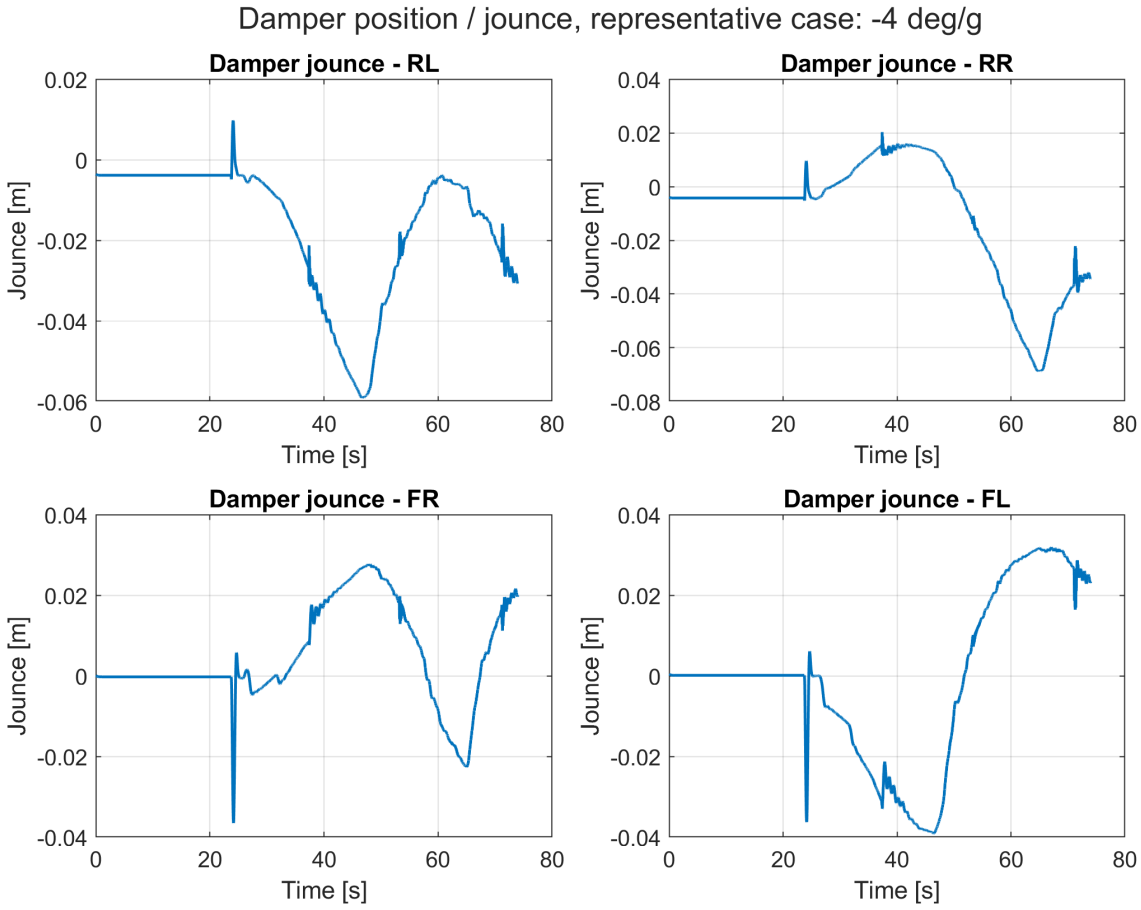

Figure A.3: Damper jounce signals at the four suspension corners for the representative -4 deg/g VI-CRT case. The subplots show the rear-left, rear-right, front-right, and front-left damper displacements, illustrating the suspension travel associated with the most demanding active roll-gradient target.

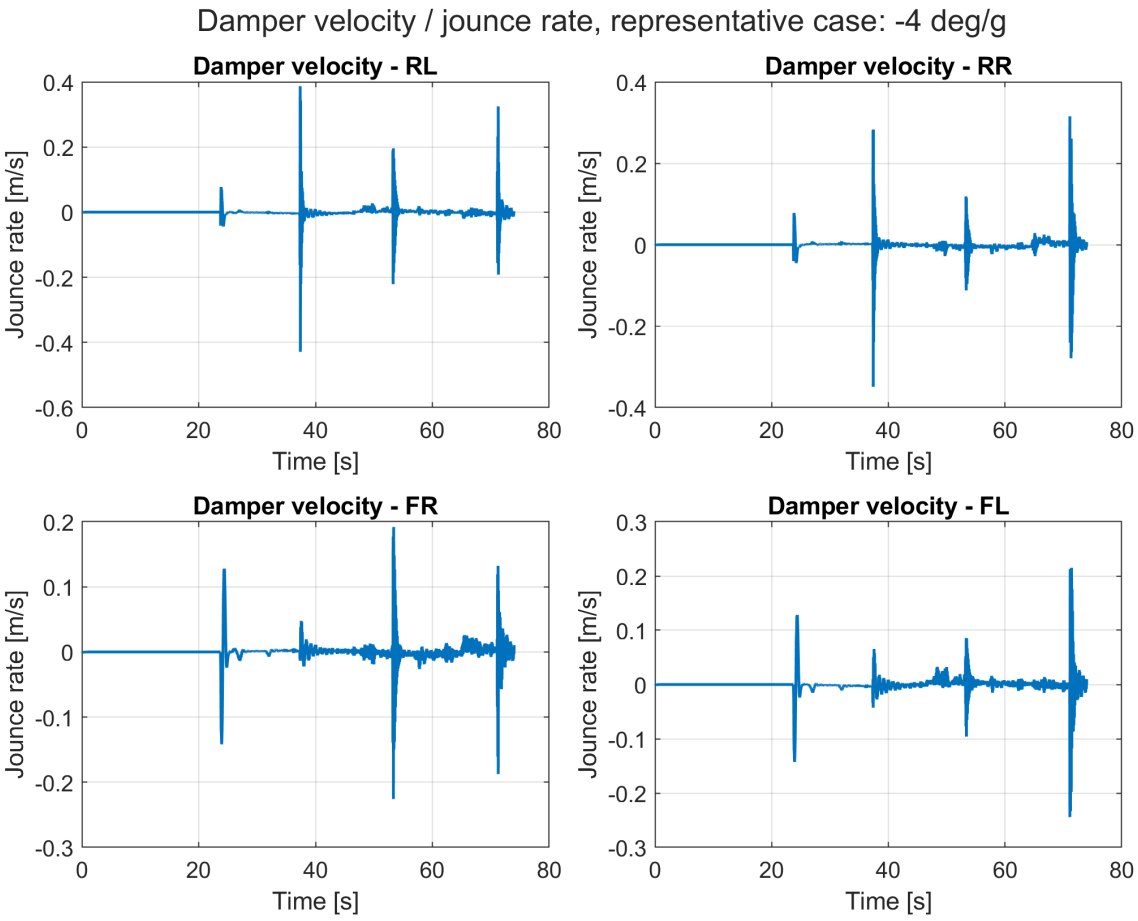

Figure A.4: Damper velocity, or jounce-rate, signals at the four suspension corners for the representative -4 deg/g VI-CRT case. These signals are relevant to the low-level actuator logic because damper velocity is used to distinguish compression and rebound behavior.

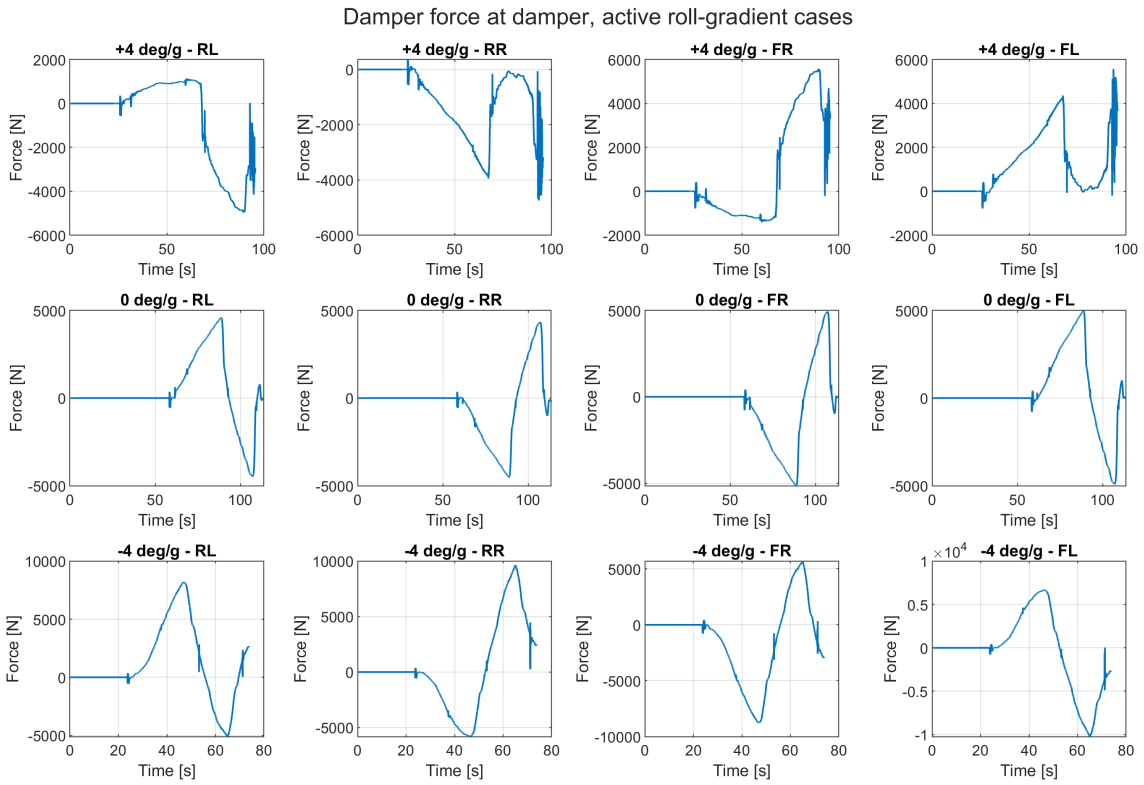

Figure A.5: Damper-force responses at the four suspension corners for the active roll-gradient cases. The rows correspond to the +4 deg/g, 0 deg/g, and -4 deg/g targets, while the columns correspond to the rear-left, rear-right, front-right, and front-left suspension corners. The figure shows how the required actuator force varies with the selected roll-gradient target.

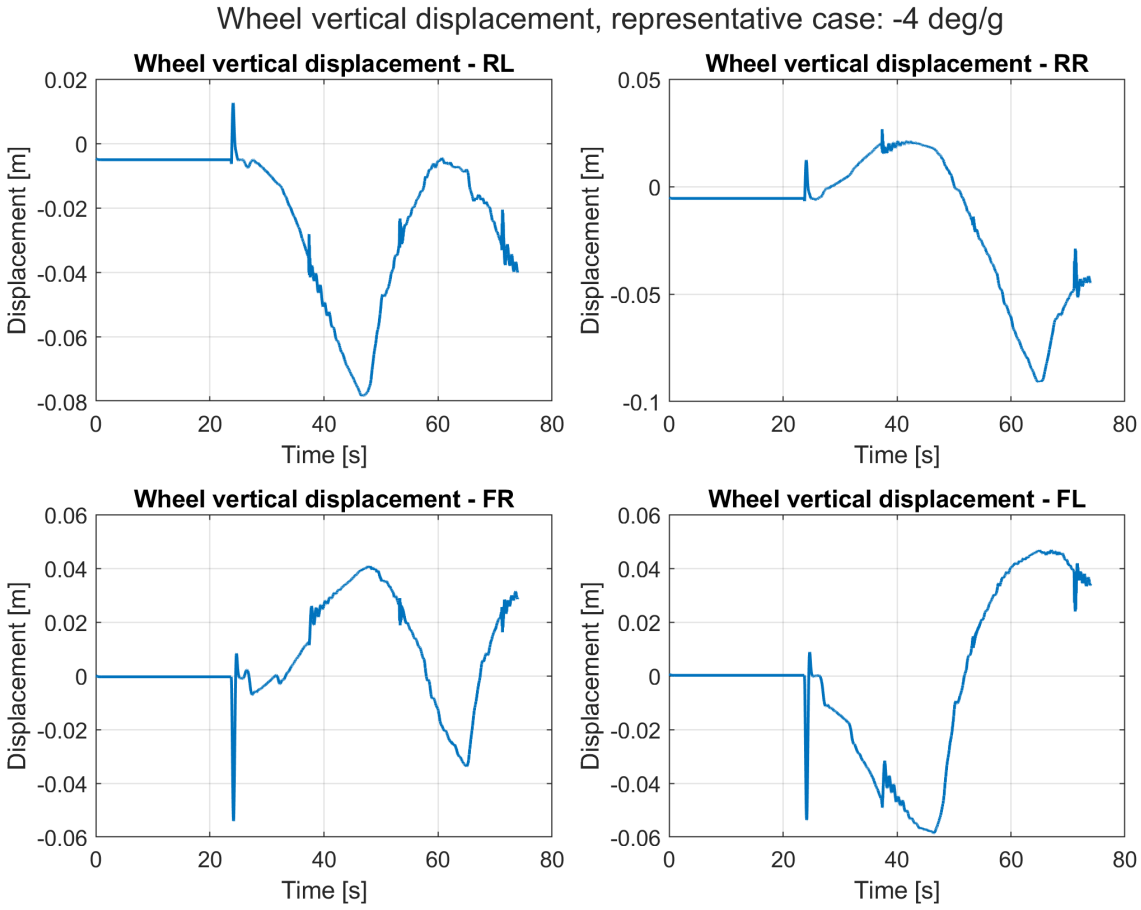

Figure A.6: Wheel vertical displacement at the four suspension corners for the representative -4 deg/g VI-CRT case. These signals complement the damper-jounce results by showing the corresponding vertical wheel-center motion during the maneuver.

Department of Mechanics and Maritime Sciences
CHALMERS UNIVERSITY OF TECHNOLOGY
Gothenburg, Sweden
www.chalmers.se

CHALMERS
UNIVERSITY OF TECHNOLOGY